出國報告（出國類別：研究）

赴美國芝加哥市參加 2009 年
大氣飛行力學研討會出國報告

服務機關：行政院飛航安全委員會
姓名職稱：張國治副飛安官、楊明浩副工程師
派赴國家：美國伊利諾州芝加哥市
出國期間：98 年 8 月 8 日至 98 年 8 月 15 日
報告日期：98 年 11 月 12 日

目次

一、目的

本次出差預算來自科發基金補助 (民國 97 年 12 月至民國 98 年 11 月)，本會擬藉執行「提升我國飛航事故調查能量」，整合國內不同領域之學界資源，以開發飛安會未來所需之調查分析能量，以協助本會找尋飛航事故調查之可能肇因。

本次投稿及參加 2009 年美國航太學會大氣飛行研討會（2009 American Institude of Aeronautics and Astronautics, Atmospheric Flight Mechanics, AIAA AFM），旨揭乃執行科發計畫核心指標－國際研討會/期刊發表論文，職擬於該研討會發表論文題目：應用降階模式分析民航機遭遇亂流之縱向飛航操作品質 (Longitudinal Flight Handling Quality Analysis by Reduced Order Motion of a Civil Transport Aircraft Encountering Turbulence)，並蒐集飛行力學及飛航資料分析相關資料。

1.1 美國航太年會大氣飛行研討會

美國航太學會當前航空太空領域中最大之學會，該學會目前擁有 35,000 名來自世界各地之會員及 90 個團體會員；該學會每年定期發布 SCI 期刊，如 AIAA Journal、Journal of Navigation Guidance and Control 及 Journal of Aircraft...等，該期刊爲當今航太領域首屈一指之期刊。該學會對航太領域之影響可由其宗旨略窺一二：

"AIAA brings together industry academica and germnment to advance engineering and science in aviation, space, and defencse"....以上摘錄自 AIAA 網頁

該學會每年舉辦超過 30 場次國際研討會，研討會議題包含：流體力學、結構力學、飛行力學、導引、導航、控制、大氣、太空科技、及通訊等航太重大議題，供全世界從事航太研究人員於此高水準之殿堂進行研討。

本次參加之大氣飛行研討會，傳統上每年皆與導引導航控制研討會 (Navigation Guidance and Control, GNC)及建模與模擬研討會(Modeling and Simulation Technology, MST)同時舉行。本年度該場研討會於 8 月 10 日至 13 日美國芝加哥市 Hyatt Regency McCormick Place 飯店舉行。研討會地點如圖 1 所示。本會人員於研討會報到區照片如圖 2 所示。

圖 1 研討會地點 Hyatt Regency McCormick Place 飯店 (資料來源 Google Map)

圖 2 本會人員於 AIAA 研討會報到處

1.2 出國行程與研討會議程

本次參與該研討會行程安排如下表 1，原預計行程於 8 月 7 日啓程，但因受莫拉克颱風侵襲臺灣，使得由桃園機場起飛之國際航班延後起飛，原班機延至 8 月 8 日凌晨 3 點左右方才起飛至洛杉磯。爲避免因颱風造成本次行程延誤，無法接上洛杉磯至芝加哥之航班，特於出發前即與航空公司票務人員接洽，更改航班。但抵達洛杉磯機場後，原訂之班機爲當地時間 8 日起飛之班機因機械故障，需要時間修復而延後起飛，該航班經多次延後仍未修復，經向該班機飛航組員詢問後，組員表示此次延誤係因該機煞車系統控制電腦(BSCU)故障無法排除，需等待一台新原件以更換，在得知該機無法起飛之原因後，當下遂即更換航班，抵達芝加哥已是當地 8 日下午 4 點多。

表 1. 參與研討會議行程

日期	行程安排
08/08 (六)	啓程：台北－洛杉磯
08/08 (六)	轉機：洛杉磯-芝加哥
08/09 (日)	準備會議資料
08/10~13(一~四)	AIAA 研討會
08/13 (四)	轉機：芝加哥-洛杉磯
08/14~15 (五)	返程：洛杉磯－台北

芝加哥在美國歷史上屬於早期開發之大城市，因此交通便利，擁有捷運、公路及鐵路運輸系統。研討會期間住宿之旅館於開會地點適合搭乘鐵路前往市區，該鐵路系統主要作爲通勤列車，作爲芝加哥郊區住民前往市區之主幹道，故於離峰時間之班次量甚少。

本次研討會共有大氣飛行研討會、導引導航控制研討會及建模與模擬研討會同時舉行。三場研討會中共發表將近 710 篇論文，其中大氣飛行研討會約 112 篇、導引導航控制研討會共 471 篇及建模與模擬研討會 127 篇。每篇文章有 30 分鐘，發表者約使用 20~25 分鐘進行發表，剩餘時間則爲自由提問。本次大氣飛行研討會共有 3 天議程議題，分別如表 2 所示。會議內容與本會業務相關之論文將於第二章中予以介紹。

表 2. 參與研討會議行程

論文主題(英)	開始時間	論文主題(中文)
Monday, 10 Aug 2009 2009 年 8 月 10 日,星期一		
AFM Student Paper Competition	0900 hrs	**大氣飛行力學研討會學生論文比賽**(09:00)
Aircraft Dynamics I	0900 hrs	飛行力學 I (09:00)
Aircraft Flying Qualities	0900 hrs	飛行操作品質 (0900)，本會論文發表於此
Mars Entry, Descent, Landing, and Return	0900 hrs	進入火星大氣載具降落落地及返回(0900)
Aircraft Aeroservoelastic Control Modeling and Optimization I	1300 hrs	飛行控制模擬及最佳化 (1300)
Projectiles and Missiles	1300 hrs	火箭及飛彈 (1300)
System Identification I	1300 hrs	系統識別 I (1300)
Vehicle Flight Test	1300 hrs	飛行測試 (1300)
Tuesday, 11 Aug 2009 (2009 年 8 月 11 日,星期二)		
Launch Vehicles and Missile	0900 hrs	載具及火箭發射 (0900)
Unmanned Aerospace Vehicles and Systems I	0900 hrs	無人太空飛行載具與系統 I (0900)
Use of UAVs in Atmospheric Flight Mechanics Education	0900 hrs	應用無人飛機進行大氣飛行力學教育 (0900)
Handling Qualities Workshop: 40 Years with Cooper Harper Scale	0900 hrs	飛航操作品質討論會- Copper Harper 量表 40 年 (0900)
Aircraft Dynamics and Control	1400 hrs	飛行力學與控制 (1400)
System Identification II	1400 hrs	系統識別 II (1400)
Workshop on Atmospheric Flight Mechanics Education	1400 hrs	大氣飛行力學教育討論會 (1400)
Wednesday, 12 Aug 2009 (2009 年 8 月 12 日,星期三)		
Aircraft Dynamics II	0900 hrs	飛行力學 II (0900)
Unmanned Aerospace Vehicles and Systems II	0900 hrs	無人太空飛行載具與系統 II (0900)
V/STOL and Rotorcraft Handling Qualities	0900 hrs	垂直起降槳葉飛機操作品質 (0900)
Aircraft Aeroservoelastic Control Modeling and Optimization II	1300 hrs	飛行控制與最佳化 II (1300)
Aircraft Dynamics III	1300 hrs	飛行力學 III (1300)
Control Methods to Meet Handling Quality Requirements	1300 hrs	飛航操作品質控制 (1300)

本計畫由飛安會副工程師楊明浩投稿於大氣飛行研討會，論文題目爲：應用降階模式分析民航機遭遇亂流之縱向飛航操作品質，論文編號爲：AIAA-2009-5610，該文於 8 月 10 日發表於第三場之飛航操作品質分析，如下圖 2。

Monday Morning / 10 August 2009							
Session 2-AFM-2 **Aircraft Dynamics I** Chaired by: S. KOMADINA, Northrop Grumman Corporation, El Segundo, CA, and M. BOLENDER, U.S. Air Force, Wright-Patterson AFB, OH							
0900 AIAA-2009-5600 Nonlinear Analytical Elucidation of Low Order Flight Dynamic Systems Using Volterra Kernels A. Omran, Old Dominion University, Norfolk, VA	0930 AIAA-2009-5601 Six- Degree- of- Freedom Simulation of Hypersonic Vehicles S. Frendreis, University of Michigan, Ann Arbor, MI	1000 AIAA-2009-5602 Improving Receiver Station- Keeping by Formulating Tanker Motion as Disturbance C. Elliott, University of Texas at Arlington, Arlington, TX	1030 AIAA-2009-5603 Modeling and Sensitivity Analysis of the Meridian Unmanned Aircraft D. Royer, University of Kansas, Lawrence, KS	1100 AIAA-2009-5604 Generation of Equations of Motion of Flying Vehicles - General Remarks K. Sibilski, Air Force Institute of Technology, Warsaw, Poland	1130 AIAA-2009-5605 5- Degree- of- Freedom Dynamic Rig for Wind Tunnel Tests of Aerospace Vehicles A. Sen, Indian Institute of Technology, Kanpur, India		

Monday Morning / 10 August 2009							
Session 3-AFM-3 **Aircraft Flying Qualities** Chaired by: R. HESS, University of California, Davis, CA, and K. SHWEYK, The Boeing Company, Huntington Beach, CA							
0900 AIAA-2009-5606 Flight Assessment of Pilot Behavior with Smart- Cue and Smart- Gain Concepts Active D. Klyde, Systems Technology, Inc., Hawthorne, CA	0930 AIAA-2009-5607 A Comparison Between Three Handling and Flying Qualities Assessment Methods M. de Koning, Delft University of Technology, Delft, The Netherlands	1000 AIAA-2009-5608 Candidate Structure for Modeling Pilot Control Behavior with Sudden Changes in Vehicle Dynamics R. Hess, University of California, Davis, CA	1030 AIAA-2009-5609 Means for Flying Qualities Improvement in Piloting Tasks Required Extremely High Accuracy A. Efremov, Moscow Aviation Institute, Moscow, Russia	1100 AIAA-2009-5610 Longitudinal Flight Handling Quality Analysis by Reduced Order Motion of a Civil Transport Aircraft Encountering Turbulence M. Yang, National Cheng Kung University, Tainan, Taiwan (roc)			

圖 2 論文發表場次

本次投稿主題爲利用民航機機載之飛航資料記錄器(Flight Data Recorder, FDR)紀錄之飛航資料，採用渦流消散率作爲亂流強度判斷指標，並應用擴展式卡爾曼濾波器(Extended Kalman Filter, EKF)提升飛航資料精度(降低 Bias 及 Noise 的影響)，透過徑向基底類神經網路學習飛機之動態模式後，進行飛機縱向運動識別相關氣動力導數，透過氣動力導數及亂流強度指標分析飛機遭遇亂流時其穩定度及操控性變化，本研究發現某型民航機穿越強烈亂流時，其氣動力之穩定導數及控制導數都會衰減，甚至造成水平尾翼的反向控制(inverse control)，並降低操作品質至 Level 3 及引起飛行員誘導振盪(Pilot Induced Oscillation, PIO)之可能性。本報告吸引非常多國外學者參與，並於論文報告後引起現場學者不少興趣及詢問，詢問之主題不外乎如何應用類神經網路架構進行飛航參數系統識別、識別結果及擴展式卡爾曼濾波器間是否會互相影響，另外還有一位美國空軍中校詢問本研究中針對飛行員於飛行過程遭於亂流時，依本研究於飛機在操控上的建議。職於研討會報告之照片如圖 3。

圖 3 本次參加 AIAA 研討會論文提報

二、會議重點

該研討會主題以載具之飛行力學、導引及導航及控制理論爲主。載具包含:飛機、飛彈、無人載具、太空載具及模擬系統之開發。此外；相關衍生議題包含:載具之氣動力識別、控制、飛航操作品質、危害天氣與飛行力學、及航管流量管制。在會場中不時可以看到各種不同國籍及膚色的人，彼此或許不相識，無論是會場內或是會場外，皆可見到熱烈討論的場景。會場中，主辦單位亦陳列美國航太學會出版之導航、系統識別及資料處理等書籍，該系列叢書對飛航資料處理及分析方法，極具參考價值。

飛行模擬器乃由動感平台、3D 場景/視效/音效模擬、操作界面、外在擾動、飛行力學…等系統組成，高度整合電腦資訊、航太、航醫及機械及電機等跨領域學門。模擬器提供一擬真環境，透過模擬器之操作可使學員提早熟悉未來之操作平台，減少學員於訓練過程中不甚損壞操作平台或操作安全，以降低訓練成本；此外，應用其仿真性，亦可作爲事故調查還原及模擬，以找出事故可能肇因。由以上可知，模擬器之優劣端視其對模擬對象之仿真程度，故本次科發計畫之子計畫 1 乃在發展事故調查工程用飛行模擬器，該模擬器爲固定式平台(fixed based)。應用事故班機飛航資料，以估算該機運動學模式，進行性能衰減分析。故本次研

討會中，主要搜集主題爲系統識別、飛行操作品質及損壞飛機性能分析及積冰與亂流對於空中交通的衝擊等議題。

2.1 系統識別

影響飛機於空間中六自由度運動運動特徵之外力與外力矩，可透過氣動力導數（aerodynamic derivatives）予以描述。因此於航空工程領域中，針對氣動力導數之估算有三種方式：

(1)分析/計算流體力學

(2)風洞量測

(3)飛行測試

第一種方式可透過計算流體力學，計算整機所受之外力，其精度易受計算流力採用分析之方法及理論假設條件限制，當載具表面具不連續面或是網格點等技術影響，其模擬環境都是基於理想下之靜態模式，風洞量測爲透過流體力學之相似理論(similarity theory)，將真實飛機透過雷諾數、速度等變因控制，將等效模型於風洞提供之風場進行靜態量測。以上兩種估算方法所估算之氣動力導數，爲靜態下之氣動力導數，無法描述飛機於高動態下之氣動力特徵，需透過飛行測試予以補足。飛行測試法將飛機動態爲一輸入-輸出之動態系統，亦即將飛行員對飛機控制面及油門之輸入飛機動態系統後，透過機載量測系統量測飛機之動態響應後，儲存於紀錄器。因此飛行測試法藉由系統識別理論，將動態響應與系統輸入之關係，予以識別。綜上所述，氣動力導數估算飛行測試法，先天上仍將受限於飛航資料量測系統、測試輸入、訊號雜訊比及資料長度。此外；識別結果仍會受到資料處理及系統識別方法限制，較爲常見之問題在於：

(1) 量測資料混合之雜訊(noise)與偏移量(bias)是否能夠移除

(2) 動態系統中存在之高階響應是否能夠識別

(3) 偶合效應存在時，識別系統是否足夠強健(robust)，找出偶合效應

也正如此，應用飛航資料進行系統識別，常久以來成爲相關學者研究主題。透過系統識別之氣動力導數，可用於模擬器氣動力導數表之修正、飛行電腦控制率修正、飛機穩定性及操作性評估。

系統識別依其分析資料所在之值域，分成時域識別及頻域識別兩大類。兩者分析之資料不同。時域識別之主要目標爲時域資料，透過多參數之輸入與輸出目標進行估算，而頻域識別法則將所有分析之輸入-輸出之時域飛航資料，先利用快速傅利葉轉換後，透過系統頻寬(bandwidth)及跨越頻率(cross over frequency)

等進行識別。因此頻域識別之結果僅能適用於某一頻帶之動態響應，其動態模型於時域之資料穩合度(fittness)較差，反之；時域識別結果能滿足時域資料，但對於部份高頻資料之穩合度較差。另外；透過頻域識別可以直接獲得系統延遲時間，於頻域中只能透過間接方式進行估算。由以上可知時域與頻域之系統識別技術各有其優缺點，端視探討問題之適用性。上述兩種方法在進行最佳化過程中，不外乎採用最小平方法及(Least Square, LS)及 Maximum Likelihood(MLE).。至於頻域系統識別理論中，NASA Aim Research Center 發展累積他們於固定翼及旋翼型無人載具之氣動力導數於頻域識別之估側技術，發展出一套分析軟體-Comprehensive Identification from Frequency Domain(CIFER)作爲分析工具，該軟體有發售商用版。

本次研討會中，共有數篇論文研討透過飛行測試方法，進行氣動力導數估算。本年度投稿學者主要是以時域進行氣動力導數識別，其中較有趣之論文爲編號 AIAA 2009-5940 及 AIAA 2009-5941，關於論文內容將分述如下：

2.1.1 論文 AIAA 2009-5940

本篇論文題目"Flight Vehicle Aerodynamic Coefficients Estimation Under Limited Measurements: New Flight-test Results", 作者爲 A. K. Sarkar 等人，作者服務於印度國防研究發展實驗室(Defense Research and Development Laboratory)，本篇論文分享之重點在於如何應用有限之真實飛行測試資料進行氣動力係數(aerodynamic coefficients)與部份氣動力導數識別法。作者使用之觀測資料包含:光學追蹤儀(electro optical tracking station)提供之航機之位置及機載加速儀與陀螺儀。並針對不同的量測資料組合與資料多寡，估算出不同之參數:

(1) C_{D0} -阻力系數估算:僅有光學追蹤儀之位置觀測量

系統觀測資料包含:斜距(Slant Range)、方位角(Azimuth)及高度(elevation)，此觀測資訊與雷達相同，但光學追蹤儀提供之資料較爲精準，其估測難度較僅用雷達資料爲低。目前作者採用 3 個光學追蹤儀基站資料，並透過擴展式卡爾曼慮波器(Extended Kalman Filter)及 Modified Bryson Frazier Smoother(MBFS)估算航機位置(x,y,z)、速度(V_x,V_y,V_z)及加速度(a_x,a_y,a_z)。接下來透過位置及速度與爬升角配合彈道分析程式及應用 Maximum Likelihood Estimation(MMLE)方法，進行阻力係數估算，估算流程圖詳圖 4，估算之 $C_{m\alpha}$ 結果如圖 5 所示。

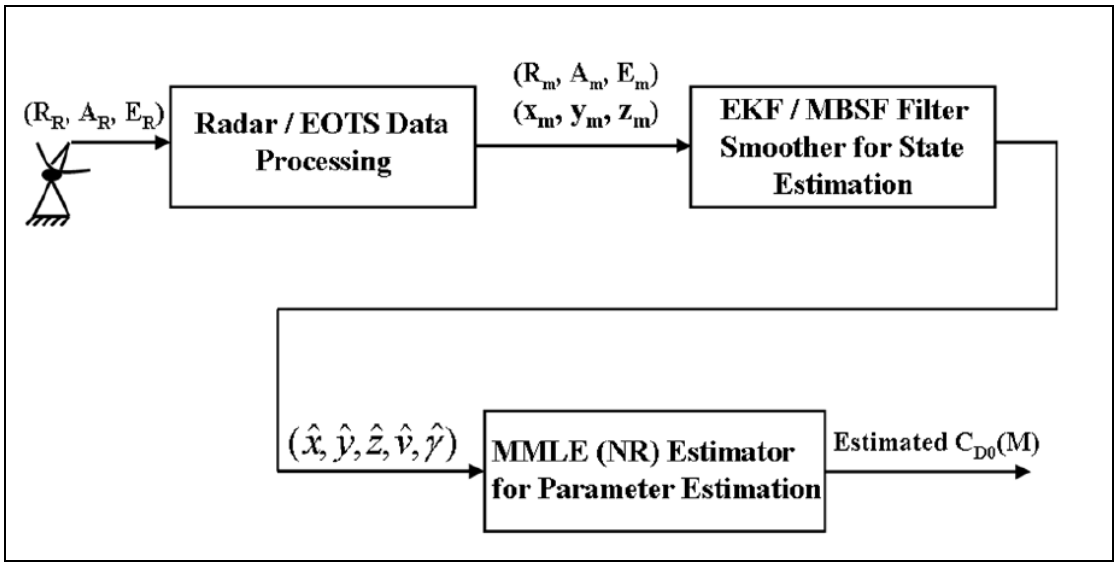

圖 4 應用雷達/光學追蹤儀進行阻力係數估算

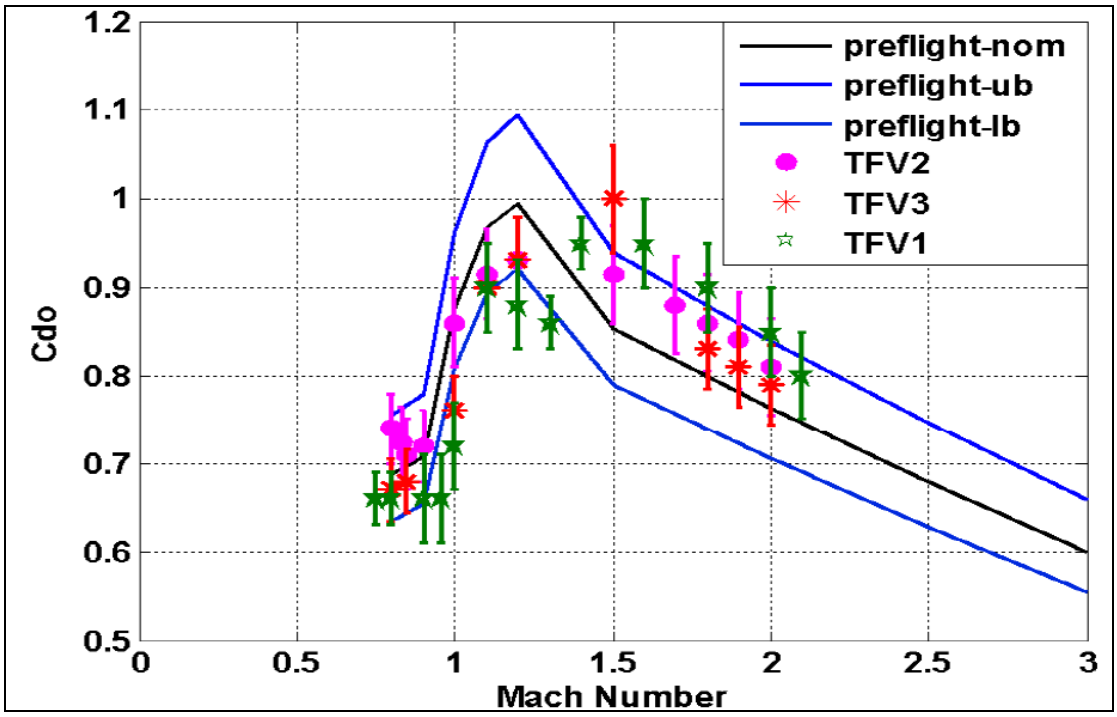

圖 5 實際估算結果

作者提醒應用此法分析時，當飛機發動機開啓時，此分析模組將受發動機推力影響甚巨，因此在缺少發動機推力模式時，將會影響即時估算結果之準確性，爲提估算之精度，可於事後將發動機之效應加入。

(2)力矩相關氣動力係數估算氣動力導數

本模組主要在如何就少數量測資料，亦可估算少數之氣動力係數。本研究僅利用機載之量測儀器提供之三軸加速儀(a_x,a_y,a_z)、三軸滾轉角速率(p,q,r)及控制面角度。作者提出兩種不同方式進行氣動力係數估算，

(a) 飛航資料結合模擬器
(b) 飛航資料直接估算法

兩者最主要的差別在於是否結合模擬器之氣動力導數。飛航資料結合模擬器之方法主要可透過模擬器提供之氣動力導數，於試飛前即可先估算出飛行狀態，以此改善若僅採用有限資料之估算方法。然而；氣動力導數數於航空公司之商業機密，即使於飛航事故調查中也不易穫得。因此本次出國報告中將不予以多述。

針對飛行料直接估算法，應用機載之三軸加速度與機軸滾轉速度，結合三座光學追蹤儀量測儀所估算之待測載具之位置與速度之外部觀測資料，利用動態匹配法採 MMLE 之估算方式，以估算三軸加速度與機軸滾轉速度之偏差，並透過擴展式率波器將系統之雜訊予以移除後即可估算氣動力係數，其估算流程如圖 6 所示。

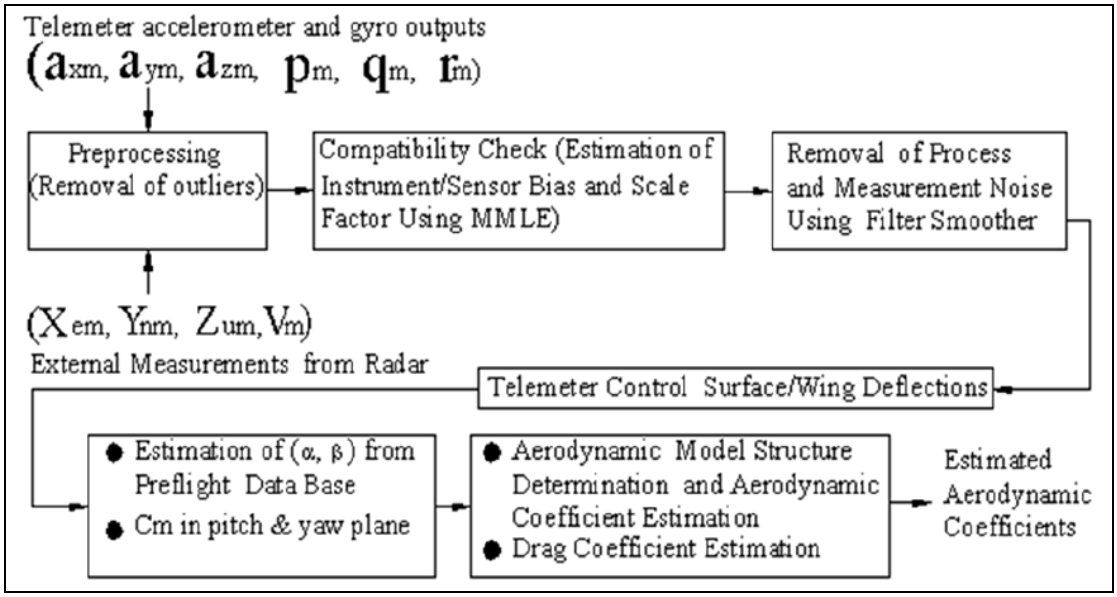

圖 6　飛航資料直接估算法

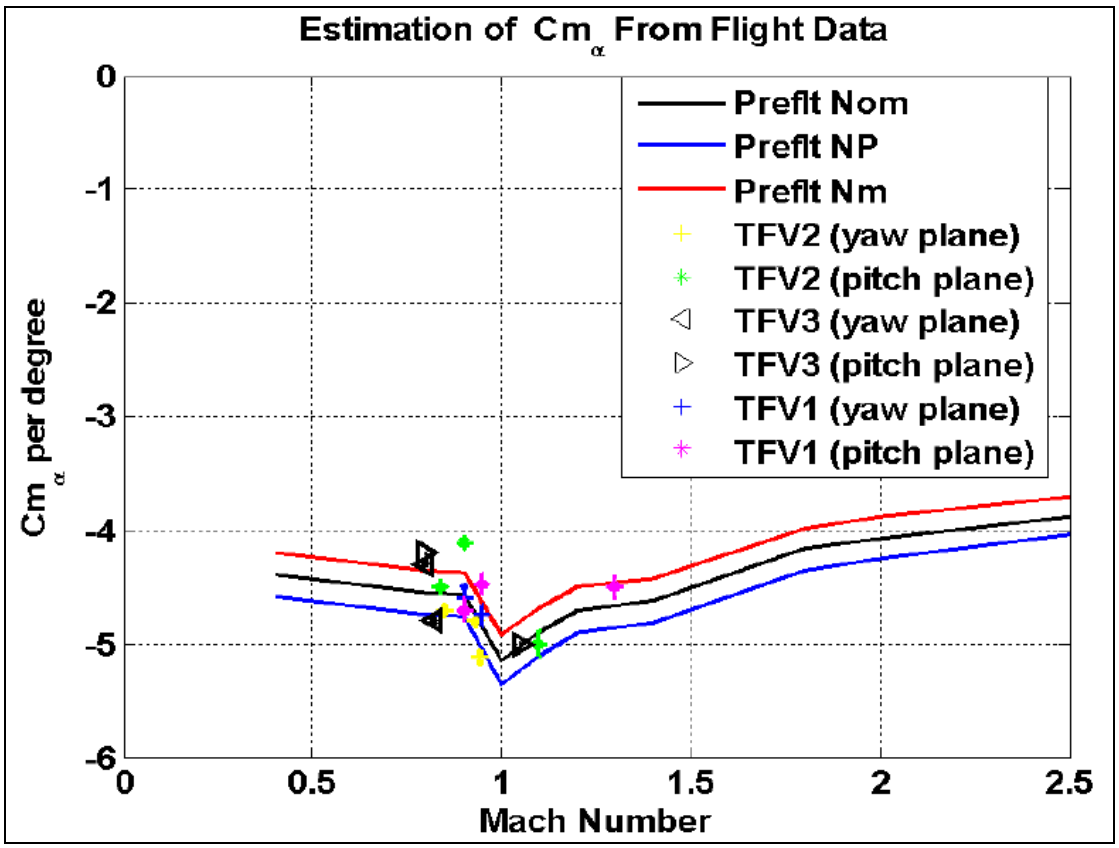

圖 7　飛航資料直接估算與模擬器比較圖

2.1.2 論文 AIAA 2009-5941

本篇論文題目"Aircraft Parameter Estimation Using Neural Network based Algotithm", 作者爲 N. K. Peyada 等人，服務於印度之 Kanpur 科技中心之航太工程部門，本篇論文使用前饋式類神經網路(feed forward neural nwtwork, FFNN)架構及 Gauss-Newton 最佳化方法，利用飛航資料直接估算氣動力導數。本研究飛航資料來自於 HANSA-3 型飛機，該機爲 4 人座之教練機，由 Kanpur 科技中心自行研發，相關性能資料如圖 8 所示。因此其概念與本會於研討會發表之論文概念接近，但採用之神精架構及估算方式有所不同。該篇論文應用前饋式類神經網路識別之結果，同時與濾波器誤差法(Filter Error Method, FEM)及最小平方法(Least Square Method, LS)進行比較。

Wing	
Span	10.47 m
Area	12.47 m^2
Fuselage	
Length	7.2 m
Weight	
Empty	485 kg
Max fuel weight	65 kg
Max T-O weigh	750 kg
Performance	
Cruise speed (at10,000ft)	116 kt
Stall speed	44 kt

圖 8 HANSA-3 型飛機基本資料

飛行力學系統識別主要是透過量測資料，將飛機運動時所遭受空氣動力及力矩透過數學方程式描述時，方程式中存在之待定系數。然而，真實世界中量測資料一定會存在雜訊及偏差值，因此估算過程中，如何處理量測資料以進行系統識別，爲相關學者一直不斷在研究主題。常使用方法有：Output Error(OE)、Maximum Likelihood(ML)及 FEM。近幾年來，透過 ML 方法，應用飛行測試紀錄之量測資料來"萃取"出飛機穩定(aircraft stability derivatives)及控制導數(aircraft control derivatives)已廣泛應用於不同之飛機試飛、測試及研究機構。然而，應用此方法進行系統識別時將會造成資料估算時之收斂及其它應用上之問題。至於採用 FEM 之方式，雖然可以處理飛航資料存在之量測及處理誤差，及應用至非線性系統架構。由於採用此法不需事先假設運動模式，及有不錯的動態資料穩合度。至於最小平方法則透過 cost function，cost function 不需定義資料之機率分佈，然而，此方法之準確度卻受量測資料之精度影響，若飛航資料之雜訊及偏差值較大，則識別結果將較差。

近幾年來，有些學者開使應用類神經網路架構透過輸入-輸出之學習機制，無需假設物理飛行模式之方法進行氣動力係數系統識別。本研究作者採用 FFNN 及 Gauss-Newton 幫法進行氣動力導數估算。

Gauss-Newton 演算法主要是應用於非線性之最小平方問題，可以視爲是 Newton's 演算法用來找尋最小值之改良法則。其估算法則如下:

給定爲 n 個變數 $\beta = (\beta_1,.....,\beta_n)$ 組成之 m 個方程式中 $r_1,.....,r_m$ ，Gauss-Newton 演算法在於找到這 m 個方程組之最小值

$S(\beta) = \sum_{i=1}^{m} r_i^2(\beta)$,其中 $m \geq n$

給予初始猜測值 $\beta^{(0)}$ ，接著可以透過疊代法

$\beta^{(s+1)} = \beta^{(s)} + \Delta$, Δ 爲一增量用來更新最小值發生時之 β ,

此增量可表示爲

$J_r^T J_r \Delta = -J_r^T r$

其中 $r = r_i$, i=1~m, J_r 是 r 對 β 的 Jacobian matrix,其維度爲 $m \times n$ 。

本研究因爲採用測試飛機進行測試，故該機可以執行某些特殊動作以便於系統識別作業。飛航資料則透過飛機上的飛航資料擷取系統，所有量測的飛航料仍須經由動態匹配(compatibility check)，並將相關量測資料處理至重心後，方才進入類神經網路系統。於類神經網路中，輸入參數

$U(k) = (\alpha(k), \theta(k), q(k), V(k), C_D(k), C_L(k), C_m(k))$

其中 $C_D(k), C_L(k), C_m(k)$ 則是由代入量測資料 a_x, a_z ,動壓(dynamic pressure),引擎推力等參數。輸出參數爲 k+1 時刻之資料，定義爲

$Z(k+1) = (\alpha(k+1), \theta(k+1), q(k+1), V(k+1), a_x(k+1), C_z(k+1))$

其神經網路架構，如圖 9 所示。

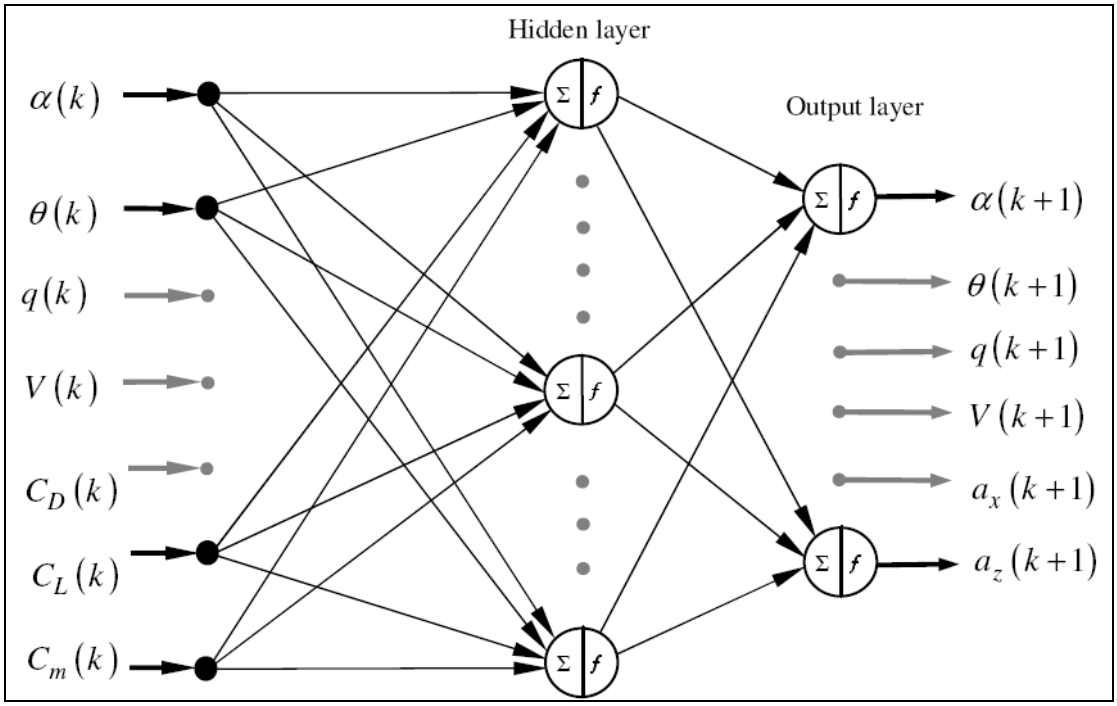

圖 9 類神經網路架構圖

就縱向運動之氣動力及力矩，假設爲下列氣動力導數所組成

$C_D = C_{D0} + C_{D\alpha}\alpha + C_{D\delta e}\delta_e$

$C_L = C_{L0} + C_{L\alpha}\alpha + C_{Lq}(\bar{q}\bar{c}/2V) + C_{L\delta e}\delta_e$

$C_m = C_{m0} + C_{m\alpha}\alpha + C_{mq}(\bar{q}\bar{c}/2V)q + C_{m\delta e}\delta_e$

因此本研究主要識別縱向之氣動力導數爲

$\Theta = [C_{D0}, C_{D\alpha}, C_{D\delta e}, C_{L0}, C_{L\alpha}, C_{L\delta e}, C_{Lq}, C_{m0}, C_{m\alpha}, C_{m\delta e}, C_{mq}]$

進行橫向氣動力導數估算時，其輸入向量

$U(k) = [C_Y(k), C_l(k), C_n(k), \beta(k), \phi(k), \varphi(k), p(k), r(k)]$

輸出向量爲

$Z(k+1) = [\beta(k+1), \phi(k+1), \varphi(k+1), p(k+1), r(k+1), a_y(k+1)]$

本研究主要識別橫向之氣動力導數爲

$$\Theta = [C_{Y0}, C_{Y\beta}, C_{Yp}, C_{Yr}, C_{Y\delta r}, C_{l0}, C_{l\beta}, C_{lp}, C_{lr}, C_{l\delta r}, C_{l\delta a}, C_{n0}, C_{n\beta}, C_{n\dot{\beta}}, C_{np}, C_{nr}, C_{n\delta r}]$$

依據該研究所獲得之氣動力導數結果，可以發現頗爲接近，其結果如圖 10 所示。但作者僅提供氣動力導數之平均值，未能提供每一量測時刻氣動力導數。然而，該方法可供本會作爲參考。

Parameter	FLT1			FLT2		
	NGN	FEM	LS	NGN	FEM	LS
C_{D_0}	0.0343 (0.0006)*	0.0343 (0.00139)	0.0349 (0.00094)	0.0353 (0.00069)	0.0352 (0.00116)	0.0359 (0.00089)
C_{D_α}	0.1991 (0.00598)	0.1952 (0.01363)	0.1827 (0.00942)	0.2388 (0.00606)	0.2489 (0.01035)	0.2311 (0.00789)
$C_{D_{\delta_e}}$	0.181 (0.00632)	0.1798 (0.01493)	0.1804 (0.00997)	0.167 (0.00703)	0.1598 (0.01202)	0.1626 (0.00908)
C_{L_0}	0.3755 (0.00238)	0.3562 (0.01051)	0.3592 (0.00395)	0.3535 (0.00314)	0.3288 (0.00747)	0.3414 (0.00473)
C_{L_α}	4.87 (0.02638)	4.9692 (0.11522)	4.6329 (0.04705)	4.9719 (0.02927)	4.994 (0.07376)	4.891 (0.04747)
C_{L_q}	21.302 (0.72701)	21.45 (2.9955)	26.481 (1.22295)	18.02 (0.88719)	19.421 (2.1665)	19.494 (1.4193)
$C_{L_{\delta_e}}$	0.3083 (0.03066)	0.4647 (0.13291)	0.5716 (0.05138)	0.2605 (0.03808)	0.5051 (0.09037)	0.4272 (0.05781)
C_{m_0}	0.1073 (0.00266)	0.1021 (0.00282)	0.0999 (0.00318)	0.1154 (0.00351)	0.1039 (0.00223)	0.1036 (0.00284)
C_{m_α}	-0.4969 (0.03717)	-0.4878 (0.03141)	-0.5304 (0.03786)	-0.4275 (0.03548)	-0.4154 (0.02168)	-0.4375 (0.02847)
C_{m_q}	-6.5781 (0.98897)	-4.7902 (0.83936)	-3.704 (0.98427)	-6.5309 (1.1446)	-6.0379 (0.66239)	-5.6789 (0.85133)
$C_{m_{\delta_e}}$	-0.9304 (0.03535)	-0.877 (0.03589)	-0.8364 (0.04136)	-1.0121 (0.0414)	-0.9039 (0.0271)	-0.8887 (0.03467)

* *Values in parentheses indicate sample standard deviation.*

圖 10 估測之縱向氣動力導數值

2.2 飛行操作品質

飛機之操作品質(handling qualities)及飛行品質(flying qualities)研究始於 Cooper 及 Harper 兩位教授提出之 Cooper-Harper Rating，至今剛滿 40 年，故於本次研討會上特別開闢一個專題探討飛行操作品質。操作品質及飛行品質之區別，一般而言兩者可視爲一體，飛行品質爲大眾所能接受之定義:"飛機之量化指標或是飛行特徵，影響飛行員是否容易及精確完成該機於某些指定任務"，易即飛機之動態反應是否容易(ease)及有效地(effectiveness)遵循飛行員的控制指令，相關之資料可參見 MIL-F-8785C 及 MIL-STD-1797A。Cook 針對操作品質與飛行

品值之區分重新定義操作品質爲:飛行員對執行飛航任務過程中，對該機短週期之響應控制指標；至於飛行品質則定義成飛行員對飛機執行命令的難易程度，因此飛行操作品質亦可以用來描述飛行員於當時操作環境下所受之壓力及工作負荷之程度。由以上，可以看出 Cook 的定義上對兩者之區分亦即爲雷同，區別僅一個探討短週期之運動。因此；一般而言，仍將此兩指標統稱爲飛行操作品質。飛行操作品質與飛行力學中提及之控制性(controlibility)與穩定性(stability)有所關連。一台飛機處於不可控情形下其飛行操作品質一定是極差，但不穩定之飛機則不一定代表該機之操作品質甚差，如飛機之橫向運動之 Spiral mode 便是一例，由於 Spiral mode 的時間常數甚大，因此飛行組員可以應付此飛機運動特徵。

爲紀念飛行操作品質 Cooper-Harper Rating 40 年，研討會特地舉行 worksop，會中邀請相關學者進行討論。與會不少學者提及雖然針對有些運動模式之探討上各研究單位有各自開發之評量標準，但追本究源皆可說是源自於 Cooper-Harper Rating。採用 Cooper-Harper Rating 表格進行飛行操作品質評估時，該表格如圖 11 所示。由該表可知，依據 Cooper-Harper 概念，飛行操作品質之指標給分標準主要是依據該機是否爲可控爲第一關卡，若在可控條件下，才探討該機是否能依其要求執行任務的程度進行分類。由於該表格乃透過文字方式進行給分及等級之敘述，往往會因各人的經驗、感覺、操作習性(high gain or low gain operator)及個性而造成誤差。會議中有學者將與分析之結果透過平均的方法進行評估，大部份學者認爲透過平均方法可能會失真，若以標準差來彌補資料分佈情形，也不恰當。大部份人在利用此法進行飛行操作品質評估，都是直接將分佈圖畫出來，並探討分佈於極端之案例。

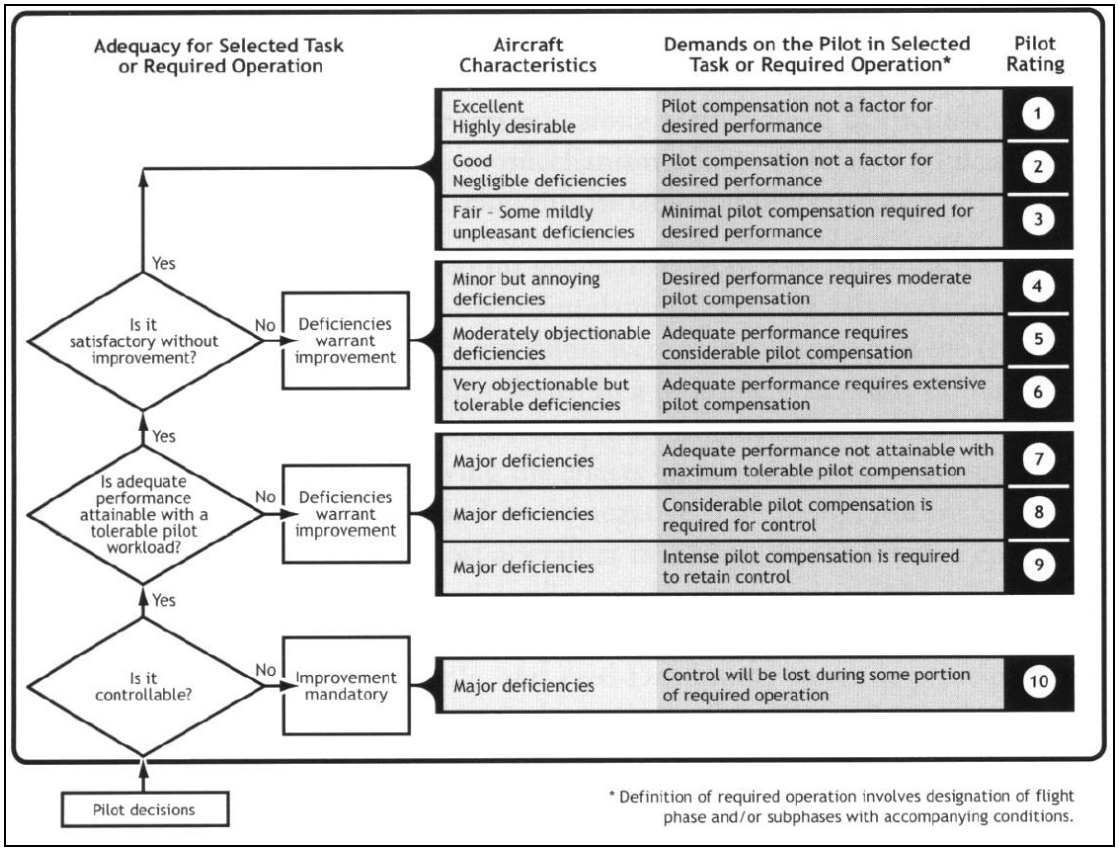

圖 11 Cooper-Harper Rating 評估標準

會議中美國 FAA 亦有出席者報告 FAA 對於民航機於設計上對飛行操作品質之要求，他提到目前 FAA 並未針對飛行操作品質特別立章節，關於民航機飛行操作品質之操作限制乃參考軍方 MIL-F-8785C 及 MIL-STD-1797A，散落於 FAR 各章節中，近日，美國 FAA 針對飛機系統零件之損壞機率及該系統損壞對飛行操控之影響，委拖相關研究機構進行研究，其成果以 AD 發出，並未強制各飛機設計公司參照此份報告。

飛行操作品質發展迄今，主要之研究方法可以分成:理論分析、模擬器及飛行測試。本次報告之論文大部份都是透過模擬器進行測試及飛行操作品質之評估辦法比較。

2.2.1 論文 AIAA 2009-5607

本篇論文作者爲 M.P de Koning,爲荷蘭 Delft University of Technology 研究生，他利用他們學校的 SIMONA 研究型模擬器-如圖 12，當採用不同評估標準下，不同之評量指標之一致性研究，他採用了 Cooper-Harper Rating(CHR)及 Handling Qualities During Tracking Method(HQDT) 及 Experimental Behavior Measurement Method(EBMM)三種評量標準進行分析。

圖 12 SIMONA 研究型模擬器

整個評估過程都需包含三個階段：

階段 1:本階段主要讓測試者熟悉及評估飛行控制器的特性，因此主要在使測試者熟悉飛機於低頻下操作特性

階段 2:本階段重點在使測試者瞭解飛機於高頻及控制器於高增益下之反應，如飛行員誘導振盪。

階段 3:本階段便開始讓測試飛行員進行任務模擬，以評估該機之操作品質。

關於 CHR 評估法則於本出國報告前節已有所述，本節將就本篇論文採用之評估方法進行探討。

Handling Qualities During Tracking Method

HQDT 評估法之發展，主要是爲了改善 CHR 在高頻或當飛機發生 PIO 時之評量方式。雖然改善試飛員操控飛機於高頻下之評比，此法仍有些許爭議。其中之一則是當試飛飛行員操控飛機於高頻響應區間時，由於多數飛行員不熟悉此區間之飛航狀態，故容易施加過量及高增益之控制輸入，因此將會造成評估結果之不準確。HQDT 之評估法則及流程請參考圖 13 所示。

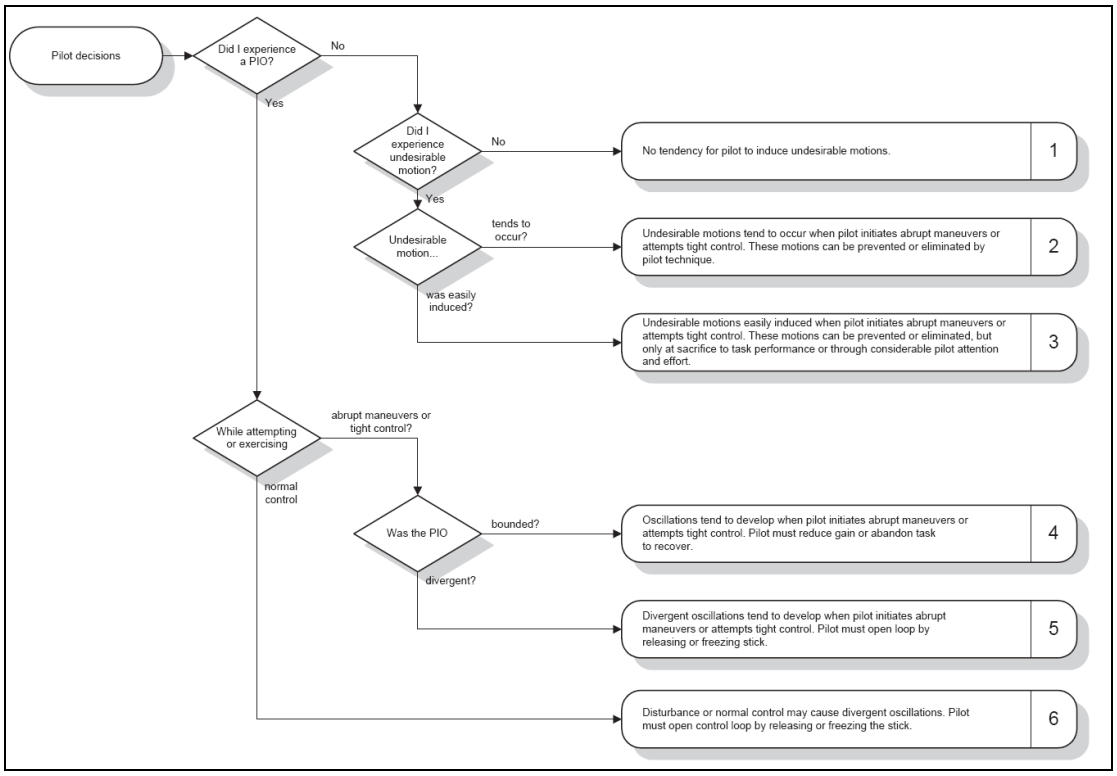

圖 13 HQDT 評估法則及流程圖

Experimental Behavior Measurement Method

EBMM 乃由 Delft University of Technology 所發展之新式指標，本方法量測飛行員對飛機之操控。因爲依據飛行操作品質之定義，本項研究之主要目地在瞭解飛行員對飛機操控之評比，故才會興起量測飛行員對飛機操控之反應作爲一科學化之證據。

EBMM 主要是飛行員追蹤一追蹤訊號，該訊號頻寬增加時，可以發現一開始飛行員將會以較大之輸入量進行控制，當頻寬增加大飛行員無法追上該訊號時，飛行員將會更改他追蹤的方式，改採低頻的方式去追蹤訊號趨勢，而 EBMM 將此一轉折頻率抓出來後，只要飛機之動態響應頻寬不應超過此一轉折頻寬。

本次實驗採用之飛機動態之設定分成三種，分別爲 Nominal aircraft(NOM), rate limited aircraft(RL)及 rate limited aircraft with anti-windup algorithm(RLAW)三種模式。NOM 模式爲一般操作模式，RL 模式爲限定飛行員對副翼輸入之速率最大爲 12.5˚/s，RLAW 除了和 RL 模式有限定飛行員對副翼輸入之速率最大爲 12.5˚/s 之外，另外還增加 anti-windup 控制率的設計，以降低當飛機發生 PIO 時，副翼輸入被鎖住之現象。本次研究採用 4 名試飛飛行員參與測試。

最後經測試及分析發現，EBMM 及 CHR 兩者在趨勢有一致性的表現，至於 HQDT 之結果與兩者不相同，詳情仍待相關人員進行更多測試後方能判斷。

2.3 損壞飛機性能分析

本篇論文編號爲 AIAA 2009-6087，作者爲 Jinwhan Kim，目前任職於 Optimal Synthesis Inc，本文作者擬透過 differential vortex lattice method(DVLM)及 Extended Kalman Filter(EKF)來估測飛機受損時，其性能衰減情形。對於外表損壞飛機而言，由於外型改變，造成飛機阻力增加及失速攻角減小，如此爲能維持飛機於何理及安全的操作下，仍維持其安全操作，作者基於此，便發展本方法。

基於簡化問題及便於估算，作者假設飛機爲點質量之飛行體，因此飛機將能依循控制器之命令維持攻角、側滑角及滾轉角固定。因此飛機之運動方程式便如下所示：

$$\dot{x} = \begin{bmatrix} \dot{V} \\ \dot{\gamma} \\ \dot{\chi} \\ \dot{x} \\ \dot{y} \\ \dot{h} \end{bmatrix} = \begin{bmatrix} (\eta T - D)/m - g\sin\gamma \\ (L\cos\phi - S\sin\phi)/(mV) - g\cos\gamma/V \\ (L\sin\phi - S\cos\phi)/(mV\cos\gamma) \\ V\cos\gamma\sin\chi \\ V\cos\gamma\cos\chi \\ V\sin\gamma \end{bmatrix}$$

相關參數說明如下

V	Velocity	Φ	Bank angle
γ	Flight angle	T	Thrust force
χ	Side-slip angle	L	Lift force
x	North	D	Drag force
y	East	S	Side force
h	Altitude	M	Mass
η	Throttle	g	Gravity acc.

依據上式之動態方程式中之升力、阻力及側向力，可透過 DVLM 進行估算，VLM 之計算基礎乃假設流體是不可壓縮，非黏滯性，穩態及非旋轉流，可以快速及有效的估算某一外型之全機氣動力特徵。於採用 VLM 估算之前，需將飛機之外型切割成許多之馬蹄型之 vortex panels，每一個 vortex pannel 都有一個 circulation 作用於 1/4 弦長之位置，如圖 14 所示。將每個 vortex pannel 加總後及可估算出飛機之升力、阻力及側向力。

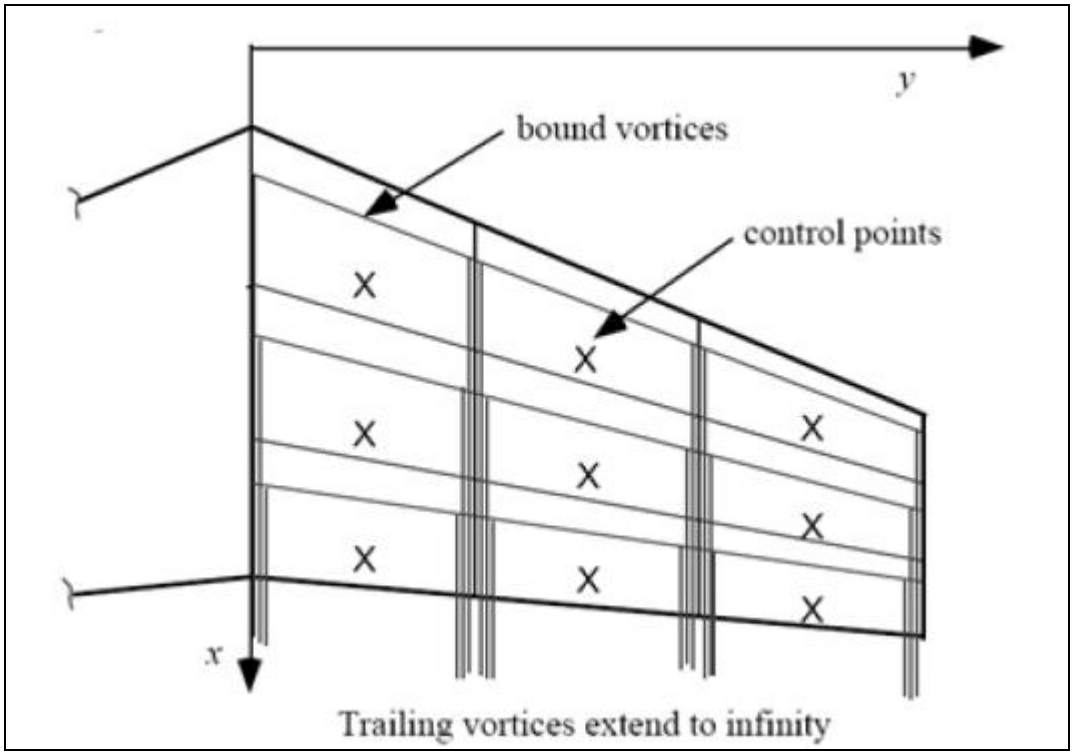

圖 14 翼面上 Vortex pannel 示意圖

本文作者假設當今飛機都有機載相機，可協助系統識別受損部位，及時估算受損後飛機性能衰減之情形，並提供控制器修正後之氣動力參數，以達即時控制維護飛行安全。

職認爲估且不論飛機破壞部位是否可辨識，相關方法可應於飛航事故調查中，分析破壞部位及該機破壞後之運動。因職並不熟悉 VLM 相關理論，故僅能作基本描述，關於本研究如何透過 DVLM 及 EKF 如何結合，請參考附件 2。

2.4 積冰與亂流對於空中交通的衝擊研究

本節共參考兩篇論文，"Modeling and Feedback of Turbulence Hazards on Automated Real-Time Pilot Reports"，論文編號爲 AIAA 2009-6066，作者爲 Gimmy Krozel，及"Impact Analysis for In-Flight Icing Hazards"，其論文編號爲 AIAA 2009-6068，作者 Shubh Krishna，兩篇論文在探討各種不同之危害天氣如霧、霾、雷暴、颱風、閃電、冰雹、大雨、積冰、下爆氣流、風切、噴流、對流亂流(Convection Induced Turbulence，CIT)、晴空亂流(Clear Air Turbulence，CAT)、山岳波(Mountain Wave Turbulence，MWT)、龍捲風、雪、火山灰等因子中，積冰與亂流對於空域之交通流量造成不同種類之限制。危害天氣對於空中交通的衝擊包含取消航班、轉降、延誤、待命、高度選擇，以及降低機場離到率。

過去相關研究曾提供駕駛員於受危害天氣影響空域飛行的指引，或是以數學模式計算危害天氣對於交通流量管理的衝擊。會議中提出積冰與亂流對於交通流量管理的影響，此研究以量化及統計的方法分析積冰、亂流與飛航管制資料，以界定這些飛航限制如何影響空域中的交通流量管理，並研究空域使用者因機冰及晴空亂流所考量之飛安及效率議題。

關於積冰，以過去 12 個顯著危害天氣資訊(SIGMET)研究量化嚴重積冰對於取消航班、轉降、延遲、待命以及降低機場離到率的影響。當 SIGMET 中，嚴重積冰影響範圍達到地面，皆造成其影響範圍或鄰近區域之主要機場航班延誤的百分比、延誤時間、以及起降航班取消顯著增加，可預測會降低空域的承載。當 SIGMET 之嚴重積冰影響範圍在地面以上，會造成主要機場航班延誤的百分比、延誤時間、以及起降航班取消增加，但程度較小，這是因爲航空器可在其影響範圍的周圍或以下的空域操作，例如飛行高度調整或空中待命，因此可避免昂貴的航班取消，但會增加駕駛員及管制員的工作負荷，以及影響 SIGMET 區域附近的空域容量，故較不可預測空域的承載降低量。然而，並不是所有嚴重積冰的 SIGMET 會顯著增加空中待命的機率。

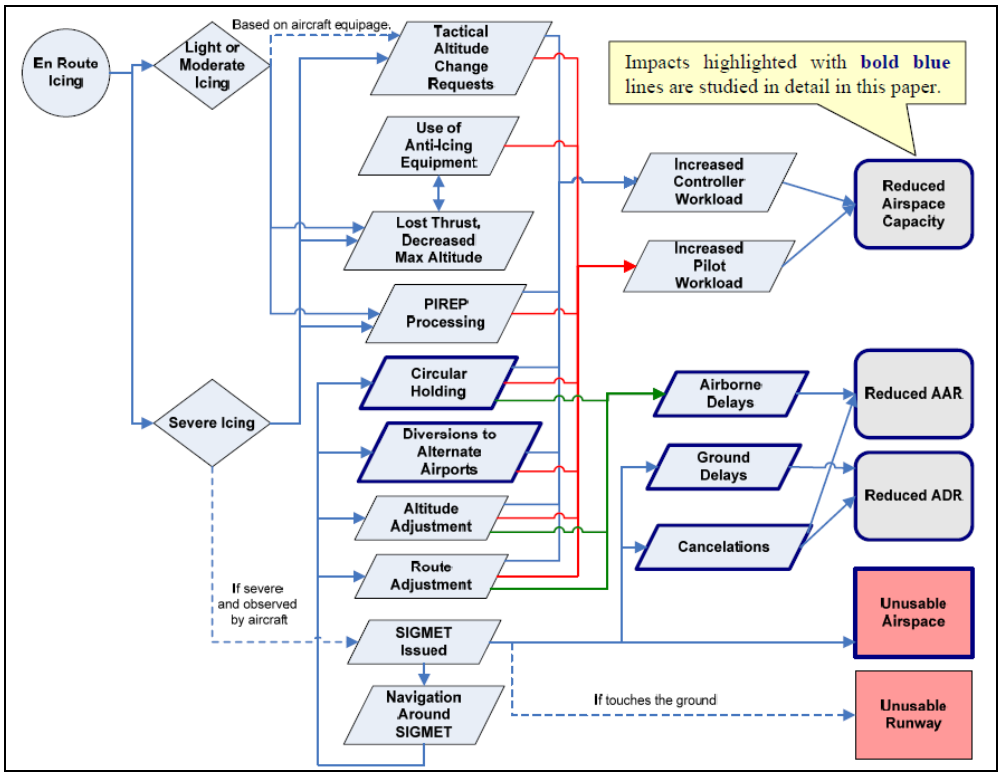

圖 15 積冰對於班機影響之示意圖

航路上之亂流是駕駛員最常遭遇的天氣因子，因爲亂流壽命較短，不容易預測其實際發生的區域。本研究係依據即時亂流自動飛報系統(Turbulence Auto-PIREP System, TAPS)所量測之亂流強度，進行飛航服務管理衝擊模式分析。此方法可應用於各類之亂流危害天氣，包括對流亂流、晴空亂流及山岳波。

本研究分析對流系統中及對流系統附近之在空機 TAPS 資料，以了解對流胞所造成之 CIT。CIT 可於強烈之對流活動中，以及其附近發生，因此駕駛員經常不知道 CIT 確實的發生位置，可能爲了躲避危害之對流天氣系統而飛入 CIT。會中並發表危害避讓模式，可以做爲首架飛入 CIT 航空器的反饋機制，提供附近之航機使用。

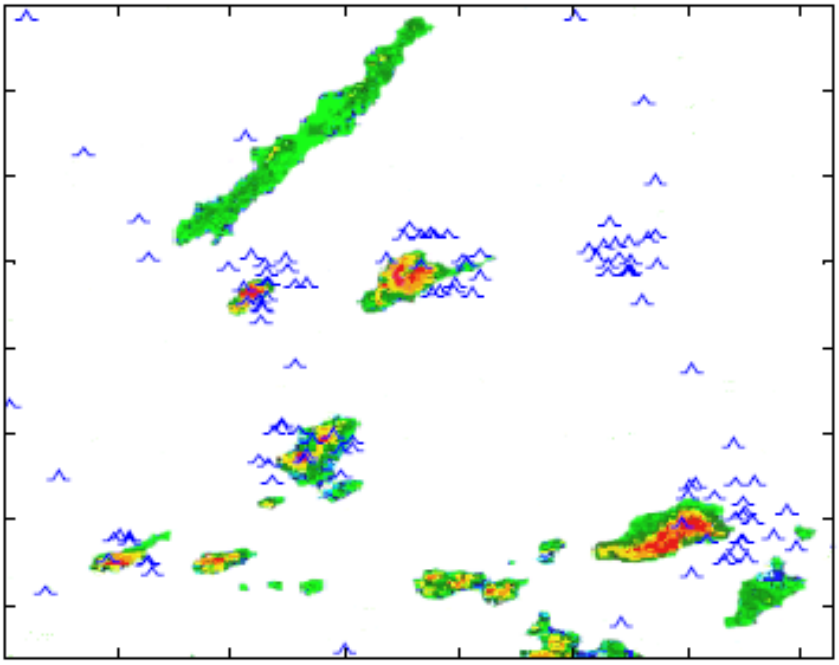

圖16 顯著對流天氣與亂流報告之示意圖

三、心得

美國航太學會舉辦之研討會，與會者來自世界各地，可稱爲高水準國際級航空研討會。本次研討會中，發現該研討會討論之主題，不僅有非常理論的控制率理論推導及煩雜數學，也有非常實務的應用性主題，未如該學會之學刊內容太過理論，不易理解甚至於應用性低。此外；本研討會包含飛行力學、大氣擾動與飛行力學、航管及模擬器等研究，與本會飛航資料之處理及從事航管調查之同仁，可以迅速獲取新知識，此行可謂收獲良多。尤其是當某些機構在報告他們單位之研究成果時，可以獲取更多及整合的資訊。除了新知獲取，亦可讓我們自省相關技術開發所採行之理論，與會學者提出之方法之優劣性，作爲本會開發人員參考。本次在研討會上，非常意外地分別遇見加拿大運輸安全委員會實驗室中負責性能分析工程師 Douglas Baker，及美國 NTSB Daniel Bower。Douglas 說 TSB 每年都會派人參加 AIAA GNC 系列研討會。

四、建議

1. 考量未來發展需求適時派員參加 AIAA 相關研討會議，吸取新知，並藉此提升我國飛航事故調查能量。
2. 參酌經費額度採購美國航太學會發行專業圖書，以供同仁參考。

五、攜回資料

研討會論文電子檔光碟一份，備份於實驗室。

六、附件

附件 1.本研究團隊發表之論文 AIAA 2009-5610
附件 2.論文 AIAA 2009-6087

附件 1 本研究團隊發表之論文

AIAA Atmospheric Flight Mechanics Conference
10 - 13 August 2009, Chicago, Illinois

AIAA 2009-5610

Longitudinal Flight Handling Quality Analysis by Reduced Order Motion of a Civil Transport Aircraft Encountering Turbulence

Ming-Hao Yang[1]
Aviation Safety Council, No. 200, Sec 3, Beisin Road, Taipei County, Taiwan, 203, Taiwan ROC
National Cheng Kung University, No.1, University Road, Tainan, Taiwan, 701, Taiwan ROC

Cjing-Shun, Ho[2]
National Cheng Kung University, No.1, University Road, Tainan, Taiwan, 701, Taiwan ROC

C. Edward Lan[3]
Kansas University, KS 66045, Lawrence, Kansas, USA

and

Fei-Bin, Hsiao[4]
National Cheng Kung University, No.1, University Road, Tainan, Taiwan, 701, Taiwan ROC

The objective of this study is to analyze aircraft's longitudinal aerodynamic characteristics and flight handling quality of short period mode by using FDR data from a civil transport aircraft encountering turbulence. The Extended Kalman Filter is used to enhance the quality of recorded data through kinematics compatibility and, at the same time, estimate some unrecorded parameters. In addition, the turbofan engine's thrust is estimated with a newly established thrust model using the FDR data; while the coefficients of aerodynamic forces and moments are evaluated with aircraft's dynamics equations. The aircraft's longitudinal aerodynamic derivatives are then estimated by a neural network method based on radial-based functions. The results for this flight show that the short period dynamic characteristic of the aircraft is stable, but the flight handling quality degrades to Level 3.

Nomenclature

CAP	=	Control Anticipation Parameter
C_L, C_D, C_m	=	Lift, Drag, and Pitching Moment Coefficient
$C_{L,D,m,x}$	=	Lift, Drag, and Pitching Moment Coefficient due to state x
EDR	=	Eddy Dissipation Rate
EKF	=	Extended Kalman Filter
NN	=	Neural Network
n_α, n_{alpha}	=	normal load factor per unit angle of attack
p, q, r	=	body rotation rate with respect to x, y ,z axis
$RBFNN$	=	Radial Based Function Neural Network
ρ	=	air density

[1] Associate Engineer / PH.D Student, Investigation Laboratory / Department of Aeronautics and Astronautics, ming-hao@asc.gov.tw.
[2] Associate Professor, Department of Aeronautics and Astronautics, csho@mail.ncku.edu.tw.
[3] Professor Emeritus, Department of Aerospace Engineering, vortex@ku.edu, AIAA Assoc. Fellow.
[4] Professor, Department of Aeronautics and Astronautics, fbshiao@mail.ncku.edu.tw, AIAA Fellow.

α = angle of attack or engine by pass ratio
δe = elevator deflection angle
δs = stabilizer for pitch trim
S = wing area

I. Introduction

In general, aircraft stability depicts whether the motion will diverge when the aircraft encounters the disturbance from its equilibrium state. The flight handling quality describes the "ride quality" for pilot to accomplish the assigned task at different flight phases. These two criteria are important for aircraft designers to verify that the aircraft is controllable without huge workload for a pilot. In any aircraft accident investigation, the investigators find the clues about flight operation, aircraft motion, and system conditions from the flight data recorder (FDR). Because of the limitation of aircraft's navigation system and the recording media capability of the FDR, sometimes there are insufficient data for investigators to perform a thorough investigation. As a result, the investigators have to utilize other tools, such as the training/engineering based simulators, for further aircraft performance and stability analysis [Ref. 1]. The training /engineering simulators are based on the certificated aerodynamic characteristics from the static wind tunnel and flight test results. These data are not capable of describing the nonlinear dynamic flight conditions in accident flight or in adverse weather encounter. Except the analysis of stability and performance, the investigators have not employed the flight handling quality in the accident investigation.

In the present study, the severity of the atmospheric turbulence is evaluated by the turbulence index (TI) or eddy dissipation rate (EDR) from the FDR data of a civil transport aircraft flight at the cruise altitude. The flight data will be filtered with the Extended Kalman Filter (EKF) to perform the kinematics compatibility check and estimate un-recorded flight data, such as the 3-dimensional wind field, sideslip angle and rotation rates at body axis…etc. The thrust force of turbofan engines will also be estimated by a thrust model using FDR recorded engine-related data. After the forces and moments of aircraft are obtained, the radial based neural network (RBFNN) is applied to model the aircraft's longitudinal aerodynamic characteristics. The study then analyzes the degradation of the aerodynamic derivatives, the stability of short period mode, and the flight handling quality variation for this case.

II. Aerodynamic Derivatives and Flight Handling Quality Estimation from Flight Data

A. The Accuracy of Flight Data

For Civil transport aircraft, the recorded flight data is measured or calculated in the navigation system, and transmitted to the data bus in the ARINC 429 format. The flight data acquisition units (FDAU) collect the data and convert them into ARINC 542, 542A, 573, 717, 747 formats and recorded. The error sources of the readout FDR data are from the characteristics, installation, calibration of the sensors, A/D conversion process, wiring configurations and readout documents. Referring to ICAO Annex 6, ED56A and ED112, the maximum tolerance range of errors for FDR data are listed in Table 1[Ref. 2].

Table 1. The error tolerance ranges for recorded flight data referring to ED112

Parameter	Accuracy	Parameter	Accuracy
Attitude	±2 deg	Normal ACC	± 0.05 g
Airspeed	±3%	Lat ACC	± 0.05 g
Ground Speed	Depend	Long ACC	± 0.05 g
Drift Angle	Depend	TAT	±2℃
Wind Speed	Depend	AOA	Depend
Wind Dir	Depend	Lat/Long	Depend

B. Aerodynamic Derivatives Estimation

Aerodynamic derivatives are used to describe the contributions of the aerodynamic forces and moments to aircraft flight dynamics. There are three methods used to estimate the aerodynamic derivatives.

Approximate mathematical model (AMM)

AMM is the simplest and least accurate method, and are often employed in the aircraft preliminary design to evaluate the flight stability. The values of the aerodynamic derivatives are estimated from mathematical formula, tables, or charts. These formula, tables or charts have been obtained from the past experiments and/or theoretical estimation and may have been digitized. The most popular sources are the Engineering Sciences Data Unit, and the USAF DATCOM.

Wind Tunnel Measurements (WTM)

In WTM, reduced scale models of aircraft are tested. With the six- component balances, the aerodynamic forces and moments in uniform wind condition in the tunnel can be measured. The tests are performed at different tunnel wind velocities (Reynolds numbers), angles of attack, and sideslip angles to simulate the aircraft static flight conditions. For the civil transport aircraft, the airframe designers are not specifically required to undertake the dynamic testing. Therefore, when an aircraft at a highly dynamic situation, the nonlinear dynamic characteristics of the aircraft may be dominant, and the static test results are unreliable to describe the dynamic situation. Recently, the rotary balance tests have been introduced in the dynamic wind tunnel tests for civil aircraft. The rotary balance test is typically conducted at a very low Reynolds number, with the results used mainly in estimating the developed spin modes of general aviation and military aircraft. In addition, dynamic aerodynamic derivatives for a civil transport have also been acquired recently through the forced oscillation test at low speeds and low Reynolds numbers. However, how useful these dynamic data are in accident flight reconstruction and in describing the aircraft response in severe atmospheric turbulence encounter is yet to be verified. Therefore, for the time being it is imperative to estimate the aerodynamic derivatives from flight data for accident flight investigation.

Flight Test Measurements (FTM)

In FTM, a parameter identification method is still needed. In the late 1960s, FTM started being developed at NASA and some flight test research centers [Ref. 3]. As the computer calculation speed and system identification technology improved, the aerodynamic derivatives identification method has also evolved in complexity. The calculation method started from the least square to the Newton-Raphson and then evolved to the Maximum Likelihood [Ref. 4]. The aerodynamics to be identified has progressed from a linear to a non-linear one. Today, the maximum likelihood is still widely used in this field [Ref. 5]. No matter which identification method is used, the estimation is mostly based on a small disturbance theory, by building up the aerodynamics from the equilibrium or trim at a specific flight condition. The aerodynamic derivatives from this method represent the quasi-steady values as the instantaneous slope at the equilibrium states. Note that abnormal flight conditions outside the flight envelope are not flight-tested, so that the flight test data are still inadequate for accident investigation.

The aerodynamic characteristics derived from the aforementioned methods are reasonable in the normal operation. When an aircraft encounters adverse weather, such as severe atmospheric turbulence, or in a loss-of-control situation, the associated aerodynamics is expected to be highly nonlinear and dynamic in nature. Therefore, an appropriate identification method must be capable of handling more complex phenomena. One such method is that based on the artificial intelligent, AI, technique [Ref. 6].

C. Flying and Handling Qualities

The flying and handling qualities of an aircraft are described as the acceptability and suitability for safe and efficient control by pilots to execute some flight tasks. These two qualities are described qualitatively and are formulated in terms of pilot opinions. From pilots' point of view, the flying quality is regarded as how well an aircraft responds to the pilot's command. The two qualities are interdependent and are probably inseparable. Therefore, the flying and handling qualities are always to be named as flight handling quality. Pilot's perception of flight handling quality of an aircraft is influenced by many factors, such as the stability, control and dynamic characteristics of the airframe, flight control system dynamics, response to atmospheric disturbance, and cockpit design. The engineering criteria of flight handling qualities include: low order equivalent system/Control Anticipation Parameter (LOES/CAP), Bandwidth, Time response, Dropback, Nichols charts and Neal-Smith. The aforementioned criteria are based on analysis in the frequency domain and transfer functions, verified on the ground based simulators and flight-tested inside the flight envelope. The present analysis focuses on the aircraft aerodynamics and flight dynamics, and flight handling quality in the encounter of atmospheric turbulence. The parameters, used to describe the motion of aircraft, are estimated from the recorded flight data to represent the real dynamic situations of the aircraft. Instead of the simulation or wind tunnel testing parameters, are derived at quasi-steady condition.

When the aircraft encounters atmospheric turbulence, the buffeting of the airframe and its effect on pitching attitude and angle of attack may cause the aerodynamics to be highly nonlinear, or in the worst situation, the aircraft

becoming unstable. In regard to the aircraft flight dynamics, the resulting aerodynamic environment may cause the pilots to lose control of the longitudinal short period mode of aircraft. Therefore, in the present study the longitudinal short period mode is analyzed based on the damping ratio and undamped natural frequency of the reduced order longitudinal equations of motion. The CAP index and normal load factor per unit angle of attack, n_α, are used to depict the degradation of the flight handling quality.

III. Methodology

In present study, the bias and noise of the recorded flight data of a civil transportation aircraft are filtered out by performing kinematics compatibility check through Extended Kálmán Filter. In this way, the unrecorded flight data, such as sideslip angle, 3-dimensional winds…etc, are derived. The severity of encountering atmospheric turbulence is diagnosed by EDR index, evaluated by flight data. Then, the thrust forces are derived from the thrust model and the FDR recorded flight data for turbofan engines. Once the flight data and thrust forces are estimated, the aerodynamic force and moment of the aircraft at body axis are derived by plugging the flight states and thrust forces into the nonlinear flight dynamic equations. The aerodynamic forces are then translated into wind axis. In most cases when aircraft encounters atmosphere turbulence, the on board passengers and flight crew surfer injuries because of rapidly bumping of aircraft in longitudinal motion. Therefore, the study focuses on the analysis of aircraft's longitudinal characteristics of motion of the aircraft. In order to analysis the degradation of longitudinal aerodynamic characteristics of aircraft, the longitudinal aerodynamic derivatives are modeled by the RBFNN. After obtaining the longitudinal aerodynamic derivatives, the damping ratio, undamped natural frequency, CAP and n_α are estimated and used to evaluate the longitudinal flight handling quality. In the following paragraphs, the Extended Kálmán filter, atmospheric turbulence strength identification, thrust model, and radial based function neural network, employed in this study, will be discussed.

A. Extended Kálmán Filter(EKF)

EKF can be applied to the nonlinear optimal estimation. It uses the system's observations/measurements and system's dynamics, and measurement's dynamics, to estimate the noise and bias embedded in the measurements and estimate system parameters. EKF applies sequential and recursive processes by linear minimum variance theory [Ref. 8]. The nonlinear stochastic differential and measurement equations map the states and measurements at time k-1 to k can be described as

$$\begin{aligned} X_K &= f(X_{K-1}, k-1) + g(X_{k-1}, k-1)w_{k-1} \quad k = 0,1,2. \\ Z_k &= h(X_K, k) + v_k \qquad k = 1,2.. \end{aligned} \tag{1}$$

where w_k and v_k denote the processing and measurement noise of the system.

The priori error covariance matrix, P_k^-, is defined as the difference between the true state (X_k) and the predicted state $(\hat{X}_k(-))$ at time k, and can be formed as,

$$\begin{aligned} P_k^- &= E\left[(X_k - \hat{X}_k(-))(X_k - \hat{X}_k(-))^T\right] \\ &= \Phi_{k-1}P_{k-1}\Phi_{k-1}^T + G_{k-1}Q_{k-1}G_{k-1} \end{aligned} \tag{2}$$

where, $\hat{X}_k(-)$ is prior estimate of the system state at k, derived from estimated state at time k-1 from state transition matix, $\Phi_{k-1} = \left.\frac{\partial f(x,k-1)}{\partial x}\right|_{x=\hat{x}_{k-1}}$. Q is the expected value of processing noise, defined as $E(w_k w_k^T)$.

The EKF uses the Kálmán filter gain, K to adjust and update the system state at time k by the $\hat{X}_k(-)$, and the system predicted measurements and measured values.

$$\hat{X}_k(+) = \hat{X}_k(-) + K(Z_k - \hat{Z}_k) \tag{3}$$

The Kálmán filter gain is a function of priori error covariance matrix, system measurement dynamic matrix, $(H_k = \left.\frac{\partial h(x,k-1)}{\partial x}\right|_{x=\hat{x}_{k-1}})$, and measurement noise $(R_k = E(v_k v_k^{-1}))$. The final expression for the gain is

$$K = P_k^- H_k^T (H_k P_k^- H_k^T + R_k)^{-1} \tag{4}$$

Through the above calculation process, the error covariance matrix is minimized to result in

$$P_k = (I - KH_k)P_k^{-1} \qquad (5)$$

The EKF program in this study is developed by ourselves with Matlab platform. The flight data are dividing into two groups: inertial data and pneumatic data. The pneumatic data are corrected by QNH to obtain the true airspeed. The estimated states about inertial system are including u, v, w, ax, ay, az, p, q, r, and, p, q, r. In order to verify that the noise and bias of estimated states are removed, the estimated results are used to re-calculate the states of aircraft by plugging them into the nonlinear flight kinematics equations, and observe whether the estimated results are converges and approaching to the recorded flight data. After the above procedures are done, the wind speed and wind direction are calculated from the difference between ground speed and true airspeed.

B. Atmospheric Turbulence Strength Identification

The atmospheric turbulence strength can be estimated by the fluctuation of vertical acceleration, eddy dissipation rate (EDR), and the vertical wind variation [Ref. 7]. The instantaneous peak and root mean square (RMS) values can be used to indicate the severity of atmospheric turbulence in these three indexes. According to ICAO and WMO documents in 2006, the automatic pilot reporting system (APRS) is based on turbulence index (TI) to define the severity of atmospheric turbulence. The value of TI is defined in terms of the instantaneous and RMS values of EDR, and the severity is related to them as follows:

Severe: TI=15 to 27, Peak EDR>0.5
Moderate: TI=6 to 14, 0.3< Peak EDR<0.5
Light: TI=1 to 5, 0.1<Peak EDR<0.3
No: TI=0, Peak EDR<0.1

EDR describes the dissipation of turbulence kinetic energy, and the value of EDR can be estimated from the aircraft response to the vertical wind in frequency domain as follows:

$$\phi_{\ddot{Z}}(f) = \left|H_{\ddot{Z}}(f)\right|^2 \phi_w(f) \qquad (6)$$

where $\phi_w(f)$ is the vertical wind component of turbulence at frequency f, and $\left|H_{\ddot{Z}}(f)\right|$ is the transfer function of aircraft response, $\phi_{\ddot{z}}(f)$ is the aircraft response in vertical acceleration. Using von Kármán's power spectral density, and the integral for the RMS, EDR(ε) can be approximated as

$$\varepsilon^2(t) = \frac{\sigma^2(t)}{0.7V^{2/3}\Gamma(t)} \qquad (7)$$

C. Thrust Model for Turbofan Engine

The aircraft for this study is equipped with PW4159 turbofan engines. The by-pass ratio (α) and the fan pressure ratio (FPR) for these engines are 4.8 and 1.73, respectively. The engine thrust in this study is calculated from a thrust model to be developed and the FDR data. The recorded data includes, engine pressure ratio(EPR), engine exhaust temperature(EGT), N1 and N2. The nozzle exit temperature is assumed to be the same as the FDR recorded exhaust gas temperature (EGT). As a result, the time lag between the pilot command, engine response, and engine health problems are ignored. The thrust force of turbofan engine is calculated by using the momentum principle with contributions from the core engine and fan section and can be shown to be,

$$\frac{T}{\dot{m}_0} = \frac{a_0}{1+\alpha}\left[\frac{V_{ec}}{a_0} - M_0 + \alpha\left(\frac{V_{ef}}{a_0} - M_0\right)\right] \qquad (8)$$

where $\dot{m}_0$ is the mass flow rate, M_0 is the flight mach number, a_0 is the flight speed, V_{ec} is the effective exhaust velocity in the core flow, V_{ef} is the effective exhaust velocity in the fan flow. These two velocities are estimated from the Eq. (9) and (10)

$$\left(\frac{V_{ec}}{a_0}\right)^2 = \frac{2EGT}{T_0(\gamma-1)}\left[\left(EPR * \frac{P_{t0}}{P_0}\right)^{(\gamma-1)/\gamma} - 1\right] \qquad (9)$$

$$\left(\frac{V_{eff}}{a_0}\right)^2 = \frac{2}{\gamma-1}\left[\left(\frac{P_{t0}}{P_0}\frac{FPR}{N_2}\right)^{\gamma-1/\gamma} - 1\right] \qquad (10)$$

P_{t0}/P_0 is the total to static pressure ratio of the free stream before entering to the engine, and T_0 is the static temperature of the free stream.

D. Radial Based Function Neural Network (RBFNN)

RBFNN is a type of feed-forward NN. The structure of RBFNN consists of 3 layers: input, hidden layer, and output layer. The hidden layer is a radial based function, and measures the distance between the input and weighted distance. The weighted distances are summed and compared to the target value. The above depictions are written as

$$y = \sum_{j=1}^{M} w_j * \phi(\|x - c_j\|) + w_0 \qquad (11)$$

where $\phi(.)$ is the radial based function, c_j is the center of the j^{th} neuron at hidden layer, w_j is the weighting, and w_0 is the bias. In this study, the Gaussian function is used as the radial based function:

$$\phi(\|x - c\|) = \exp\left[-\frac{\|x-c\|^2}{2\sigma^2}\right] \qquad (12)$$

where σ is standard deviation, defined the shape of the radial based function.

In the learning process of the RBFNN, w_j, c_j, and σ in Eq. (13) have to be corrected with the learning rate to minimize the learning error.

$$\begin{aligned}
\Delta w_j(p) &= \eta_1 e(p)\phi(\|x(p) - c_j(p)\|) \\
\Delta c_j(p) &= \eta_2 \frac{w_j(p)e(p)}{\sigma_j^2(p)}\phi(\|x(p) - c_j(p)\|)(x(p) - c_j(p)) \qquad (13) \\
\Delta \sigma_j(p) &= \eta_3 \frac{w_j(p)e(p)}{\sigma_j^3(p)}\phi(\|x(p) - c_j(p)\|)(x(p) - c_j(p))^2
\end{aligned}$$

E. Decoupled Longitudinal Equations of Motion

Basically, the linearized decoupled aircraft longitudinal dynamics are described by the following three equations of motion as Eq. (14):

$$\begin{aligned}
m\dot{u} - \overset{o}{X}_{\dot{w}}\dot{w} &= \overset{o}{X}_u u + \overset{o}{X}_w w + (\overset{o}{X}_q - mW_e)q - mg\theta\cos\theta_e + \overset{o}{X}_\eta \eta \\
m\dot{w} - \overset{o}{Z}_{\dot{w}}\dot{w} &= \overset{o}{Z}_u u + \overset{o}{Z}_w w + (\overset{o}{Z}_q - mU_e)q - mg\theta\sin\theta_e + \overset{o}{Z}_\eta \eta \qquad (14) \\
I_y\dot{q} - \overset{o}{M}_{\dot{w}}\dot{w} &= \overset{o}{M}_u u + \overset{o}{M}_w w + \overset{o}{M}_q q + \overset{o}{M}_\eta \eta
\end{aligned}$$

where the X, Z, and M are the axial force for the drag, normal force and pitching moment, respectively. The subscript states for the $\overset{o}{X}$, $\overset{o}{Z}$ and $\overset{o}{M}$ are the dimensional aerodynamic derivatives related to the states on body axes. With M defined in the following, Equation (14) is multiplied by M^{-1} and rearranged in form of $\dot{x}(t) = Ax(t) + Bx(t)$ to result in

$$M = \begin{bmatrix} m & -\overset{o}{X}_{\dot{w}} & 0 & 0 \\ 0 & (m - \overset{o}{Z}_{\dot{w}}) & 0 & 0 \\ 0 & -\overset{o}{M}_{\dot{w}} & I_y & 0 \\ 0 & 0 & 0 & 1 \end{bmatrix}, \begin{bmatrix} \dot{w} \\ \dot{q} \\ \dot{\theta} \end{bmatrix} = \begin{bmatrix} z_w & z_q & z_\theta \\ m_w & m_q & m_\theta \\ 0 & 1 & 0 \end{bmatrix}\begin{bmatrix} w \\ q \\ \theta \end{bmatrix} + \begin{bmatrix} z_\eta \\ m_\eta \\ 0 \end{bmatrix}\eta \qquad (15)$$

where z_w is defined as coinsine form of aerodynamic derivatives. The short period mode is typically a damped oscillation in pitch about the body y-axis in normal flight conditions. The majority motion variables are including the angle of attack, pitch rate and pitch angle. If we assume the aircraft is in steady level flight, therefore, the equation of motion is represented as Eq. (16).

$$\begin{bmatrix} \dot{w} \\ \dot{q} \end{bmatrix} = \begin{bmatrix} z_w & z_q \\ m_w & m_q \end{bmatrix} \begin{bmatrix} w \\ q \end{bmatrix} \quad (16)$$

Eq. (16) is similar to a second-order vibration equation, with the natural frequency and damping ratio given by

$$\omega_{sp} = \sqrt{(m_q z_w - m_w z_q)}, \; 2\zeta_{sp}\omega_{sp} = -(m_q + z_w) \quad (17)$$

The short period transfer functions describing the pitch rate, angle of attack, and normal acceleration response to elevator control input are given by (Eq. (18), (19) and (20))

$$\frac{\dot{q}(s)}{\eta(s)} = \frac{m_\eta s(s - z_w)}{(s^2 - (m_q + z_w)s + m_q z_w - m_w z_q)} \quad (18)$$

$$\frac{a_z(s)}{\eta(s)} = \frac{m_\eta z_w u_0}{(s^2 - (m_q + z_w)s + m_q z_w - m_w z_q)} \quad (19)$$

$$\frac{\alpha(s)}{\eta(s)} = \frac{\frac{z_\eta}{u_0}(s + u_0 \frac{m_\eta}{z_\eta})}{(s^2 - (m_q + z_w)s + m_q z_w - m_w z_q)} \quad (20)$$

For flight handling qualities criteria, the normal load factor per unit angle of attack (n_α) and CAP are defined as Eqs. (21) and (22)[Ref. 12].

$$n_\alpha = \frac{n_z(t)}{\alpha(t)}\Big|_{ss} = -\frac{z_w u_0}{g} \equiv \frac{u_0}{gT\theta_2} \quad (21)$$

$$CAP = \frac{\dot{q}(0)}{n_z(\infty)} = -\frac{g\omega_{sp}^2}{z_w u_0} = \frac{g\omega_{sp}^2 T_{\theta_2}}{u_0} \quad (22)$$

IV. Numerical Results

A. Turbulence Strength Identification

The time window is 5 seconds for RMS of EDR. The instantaneous peak and RMS of EDR are denoted by EDR_{INST} and EDR_{RMS} spatially. The results are shown in Fig. 1. They show that the aircraft first time encounter turbulence is encountered at 240~270 seconds. The most severe turbulence at the first time is at 256 seconds. At that time, the EDR_{INST} is 0.557, the EDR_{RMS} is 0.436, and the TI is 19. Therefore, the flight encountered severe turbulence.

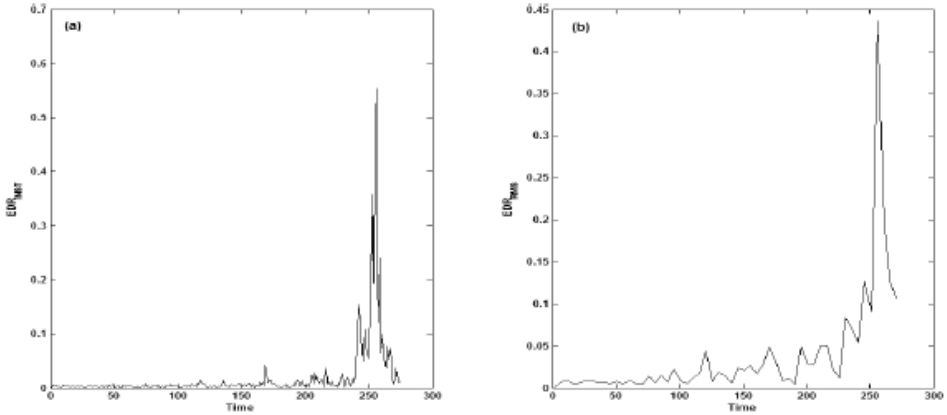

Figure 1. a) The instantaneous peak value of EDR, b) The RMS of EDR

B. Estimation of Flight Data and Thrust Force

To estimate the un-recorded flight data and remove the noise and bias of the recorded flight data, the EKF is performed as kinematics consistency in present study. The state transition and measurement matrix for EKF are the partial differential equations of nonlinear kinematics equations of flight dynamics. The thrust force is estimated by inserting the FDR recorded flight data and the dimension of the engine into Eqs. (8),(9) and (10) of the thrust model. Then the aerodynamic coefficients are estimated from the dynamic equations of motion. The time histroy for lift coefficient(C_L), drag coefficient(C_D), side force coefficient(C_Y), pitching moment coefficient(C_m), rolling moment coefficient(C_l) and yawing moment coefficient(C_n) are shown in Fig. 2.

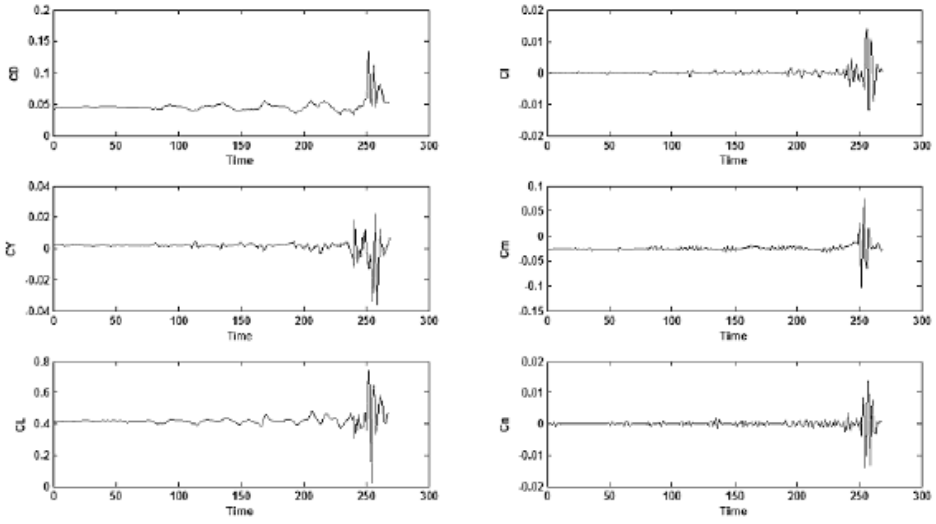

Figure 2. Variation of aerodynamic coefficients with time

Fig. 3 is the 3-dimensional wind field along the flight track. According to these calculated 3-dimensional wind field, the minimum and maximum values of wind speed normal to the horizontal plane are –9.8 knots; and 36 knots, respectively (see Fig. 3).

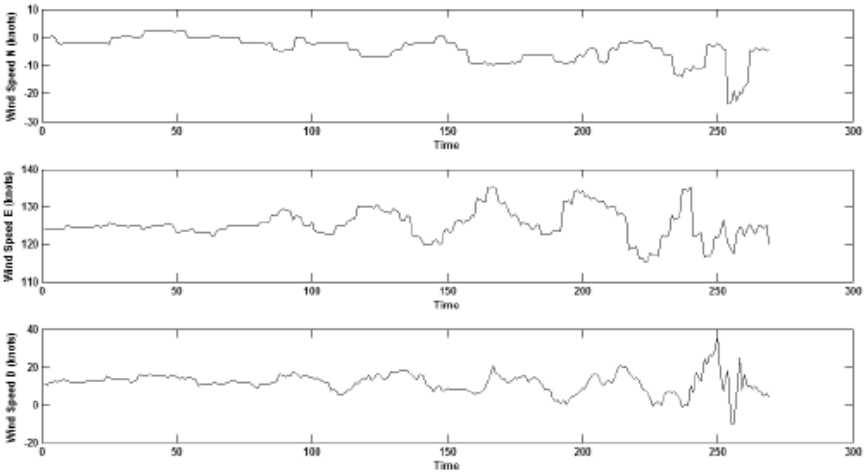

Figure 3. Estimated results for the 3 dimensional wind field

C. Aircraft Longitudinal Aerodynamic Derivatives

In the present study, the aerodynamic derivatives in the wind axes instead of body axes are estimated based on the NN models of coefficients and evaluated with a central difference scheme. Because the actual aerodynamic derivatives for the subject airplane are not available, the following results based on wind-tunnel testing for the Convair 880 and Boeing 747 and listed in Table 3 [Ref. 13] will be used for comparison, since the weight of the subject aircraft falls between these two types of aircraft.

Table 3. Some the longitudinal aerodynamic derivatives of Convair 880 and Boeing 747 (Ref. 13)

Convair 880						
	$C_{L\alpha}$	$C_{D\alpha}$	$C_{m\alpha}$	$C_{m\dot{\alpha}}$	C_{mq}	$C_{L\dot{\alpha}}$
Ma=.8	4.8	0.15	-0.65	-0.57	-4.5	0.19
Boeing 747						
Ma=.9	5.5	0.47	-1.6	-1.2	-25	0.3

The derivatives of longitudinal aerodynamic forces coefficients are assumed to be functions of Mach number (Ma) 、time rate of magnitude of vertical wind component(w_w), rotational rates of body axes (p,q,r) and its time rates($\dot{p},\dot{q},\dot{r}$), angle of attack (α) and its rate $(\dot{\alpha})$, sideslip angle (β) and its rate $(\dot{\beta})$, and the stabilizer for pitch trim (δ_e). The elevator effects on C_L and C_D are ignored. On the other hand, for the pitching moment related derivatives, the elevator deflection is considered as an important contributing variable. The longitudinal aerodynamic coefficients dut to these variables are estimated by RBFNN. The longitudinal aerodynamic derivatives will be considered below for the evaluation of the stability and flight handling quality.

In the estimation process, a quarter of the whole flight data are used in the learning process, and then the whole flight data are used to validate whether the learning results of NN represents the aircraft flight dynamics. For the optimization process of the RBFNN, the network has to update the centers of radial functions, and weightings. These values also affect the learning results. The non-linearity of RBFNN is controlled by the number of centers, and when the numbers of center are increased, the learning results will be mired in the local minimum of the learning error. Therefore, in this study, the initial value of centers of radial function and weightings are determined by the Fuzzy C-Means algorithm for the derivatives of lift and drag coefficients. The initial values of centers of radial function and weightings are determined by the orthogonal least square method for pitching moment derivatives.

Derivatives of Lift Coefficient

Before encountering atmospheric turbulence, the subject aircraft was operating normally in cruise conditions. The flight level was 330, and the Mach number was 0.78. Before encountering atmospheric turbulence, the average values of $C_{L\alpha}$, $C_{L\dot{\alpha}}$, $C_{L\beta}$ and C_{LMa} are 4.47, 0.189, -0.016, and -0.0098 respectively. Compared to the results in Table 3, the values of $C_{L\alpha}$ and $C_{L\dot{\alpha}}$ for Convair 880 are 4.8 and 0.19 at Mach 0.8, and the values for Boeing 747 are 5.5 and 0.33. Therefore, the estimated results are reasonale and are in the range for these two types of aircraft in cruise conditions.

When the subject aircraft flew into the atmospheric turbulence, $C_{L\alpha}$ varies from 5.17 to 0.41. The value of $C_{L\dot{\alpha}}$ varies from 0.189 to 0.001. From the above results, the effecitness of lift force due to stabilizer for this case is decreasing. Therefore, the control power of the stabilizer, $C_{m\dot{\alpha}}$, is expected to decrease as well. The estimated results of aerodynamic derivatives are shown in Fig. 4.

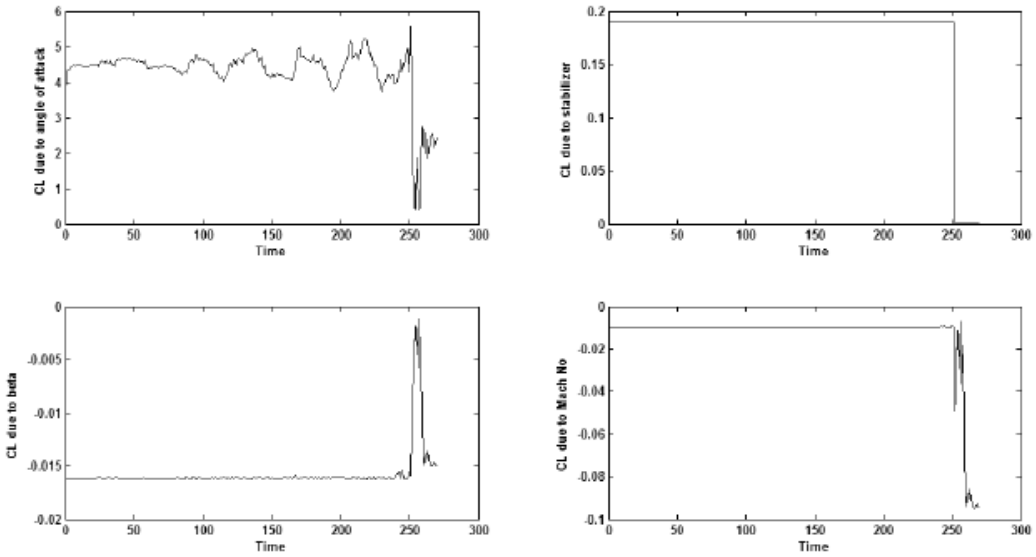

Figure 4. Some of the lift coefficient related aerodynamic derivatives estimated by RBFNN

Derivatives of Drag Coefficient

Before encountering the atmospheric turbulence, the average values of $C_{D\alpha}$, $C_{D\dot{\alpha}}$, and $C_{D\beta}$ are 0.48, 0.0001 and -0.003 respectively. In Table 3, the values of $C_{D\alpha}$ for Convair 880 and Boeing 747 are 0.15 and 0.47 respectively at Mach number 0.8. Therefore, the estimated results are in the range for these two types of aircraft in cruise conditions. The maginitude of drag derivatives are also very samll except for $C_{D\alpha}$. Therefore, these small terms are neglected in the following study.

With the aircraft in atmospheric turbulence, the values of $C_{D\alpha}$ varied in the range of 0.6 to 0.28. The drag coefficient derivative with stailizer angle is not significant.

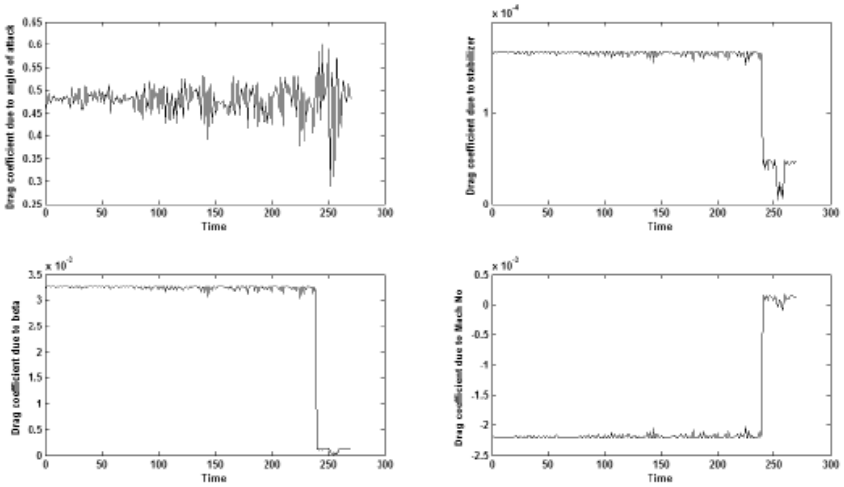

Figure 5. Some of the drag coefficient related aerodynamic derivatives estimated by RBFNN

Derivatives of Pitching Moment Coefficient

Figure 6 is some estimated derivatives of the pitching moment coefficient. Before encountering atmospheric turbulence, the average value of $C_{m\alpha}$ is -0.337; $C_{m\dot{\alpha}}$ is -2.79; $C_{m\delta e}$ is -1.12, and C_{mq} is -5.56. In Ref. 12, $C_{m\delta e}$ is -0.58 at Ma=0.8 for Convair 880, the value for the Boeing 747 is -1.2. When the aircraft encountered atmospheric turbulence, the values of $C_{m\alpha}$, $C_{m\dot{\alpha}}$, and $C_{m\delta e}$ ranged from -0.02 to -0.44, -2.92 to -0.05, and -1.64 to 0.11 respectively.

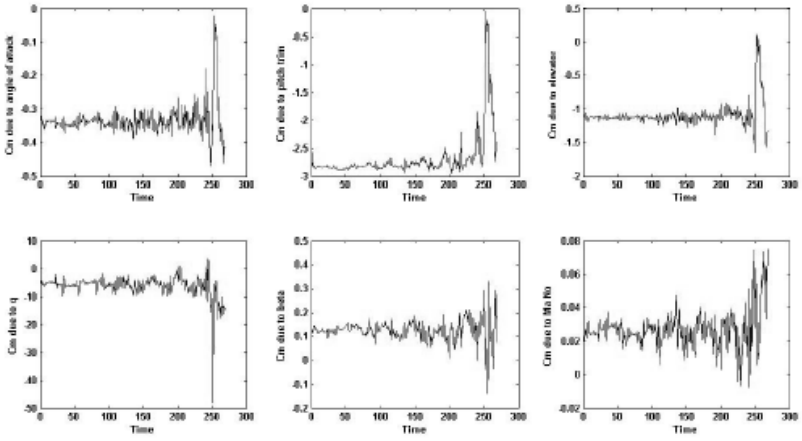

Figure 6. Some of the pitching moment coefficient related aerodynamic derivatives estimated by RBFNN

The pitching moment coefficient due to angle of attack represents the static stability of aircraft, the value being negarive in normal operation. In the severe atmospheric turbulence under consideration, although the aircraft is still statically stable, the static stability is decreasing and degraded by up to 96%. In addtion, $C_{m\dot{\alpha}}$ and $C_{m\delta e}$, representing the picting control power from stabilizer and elevator, also decreased in magnitude. In the present study, the sign for $C_{m\delta e}$ is changed from negative to positive, and referring to the Eqs. (18-20), the sign change of $C_{m\delta e}$

means that the a significant opposite phase delay of elevator control relative to the motion. If the pilot applies control to the aircraft at this moment, the motion from pilots' control to the aircraft would be oppsite to what is needed. In the worst situation, this phonemenon may cause "pilot induced oscilation".

D. Aircraft Stability and Flight Handling Quality Analysis

The aerodynamic derivatives listed in Eq. (16) are based on body axis. Except for the pitching moment derivatives, the aerodynamic force derivatives, estimating from the RBFNN in the present study, are based on wind axis. Therefore, the lift and drag derivatives have to be transformed into the body axis. In addition, the derivatives due to w and $\dot{w}$ are replaced by the derivatives due to α and $\dot{\alpha}$ by using $\Delta\alpha = w/u_0$. In addition, the aerodynamic derivatives due to axial velocity on wind axis are functions of aerodynamic foroce coefficient and the force coefficient derivative with Mach number, and the Mach number itself. For example, the lift derivative due to axial velocity is can be represented as Eq. (22),

$$L_u^o = \frac{\partial(1/2\,\rho u_0^2 S C_L)}{\partial u} = \rho u_o S C_L + \frac{1}{2}\rho u_o S \frac{1}{M_0}\frac{\partial C_L}{\partial M} = \rho u_o S C_L + \frac{1}{2}\rho u_o S \frac{1}{M_0} C_{L_M} \qquad (22)$$

According to the definition of flight phases in flight handling quality, the subject aircraft in cruise conditions should belong to Category B. After obtaining the aerodynamic derivatives on the body axis, the undamped natural frequency and damping ratio can be obtained from Eq. (17) and plotted as shown in Fig. 7. The positive damping ratio in the present study represents the stable damping (Fig. 7b). Therefore, the eigenvalues of the short period motion are on the left hand side of the imaginary axis, and the aircraft short period mode is stable in the atmospheric turbulence. Before encountering turbulence, the average value of undamped natural frequency is 2.01 (rad/sec), and the average value of the damping ratio is 0.334. In the present atmospheric turbulence, the variation of undamped natural frequency ranges from 0.43~2.55(rad/sec), and the damping ratio ranges from 0.09~1.42. Refering to the thumprint, Fig. 7c, when the aircraft is in the present turbulence, the flight handling quality in these period of time is un-acceptable because of the low undamped frequency or damping ratio[Ref. 14].

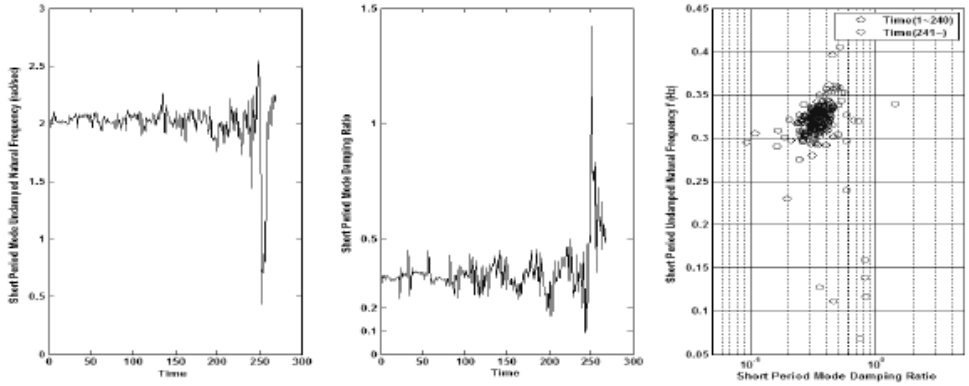

Figure 7. a)The undamped natural frequency, b) damping ratio, and c) thumb of print criteria for short period longitudinal motion

Figure 8 consists of a) CAP and damping ratio of short period mode, and b) undamped natural frequency and normal load factor per unit angle of attack. Before encountering the turbulence, The average vaule of CAP is $0.387(g^{-1}sec^{-2})$, and the average value of normal load factor per unit angle of attack is 17.51 (g/rad). The flight handling quality belongs to level 1 based on CAP and n_α . The Level 1 flight handling quality means the flight situation is clearly adequate for the mission flight phase. As encountering the atmospheric turbulence, CAP ranges from $2.21(g^{-1}sec^{-2})$~$0.13(g^{-1}sec^{-2})$, and the value of n_α ranges from 0.186(g/rad)~22(g/rad). When the CAP is $0.13(g^{-1}sec^{-2})$ and the damping ratio is 0.198. At that moment, the flight handling quality belongs to Level 3 and very closes to the Level 2. When n_α is 6.62(g/rad) and the undamped natural frequency is 0.736, the worst flight handling quality situation for this case, the handling quality belongs to Level 2 & Level 3. The Level 2 is adequate

to accomplsh the mission, but it increases the pilot workload. The level 3 flight handling quality means the aircraft is still controllable, but has inadequate mission effectiveness, and may cause the high workload for pilots.

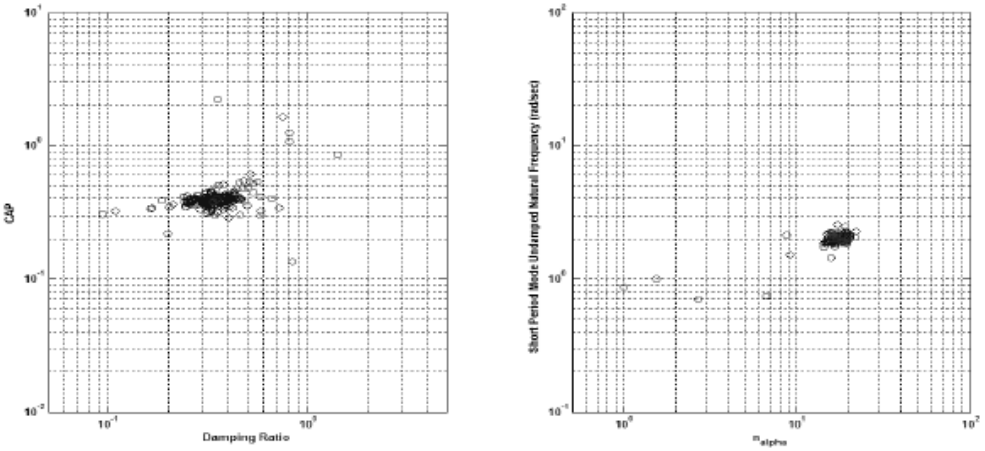

Figure 8. The short period mode of a) combining CAP and damping ratio, b) undamped natural frequency and normal load factor per unit angle of attack

V. Conclusions

From the above analysis results, the severe atmospheric turbulence caused the aerodynamics, static stability, dynamic stability, and flight handling quality degradation. The aerodynamic degradation in C_{L_α} was up to 90%, the static stability C_{m_α} was up to 96%, compared to the normal flight in cruise conditions. The most significant finding in this case was the control power reduction of the control surfaces, including the stabilizer and elevator. In particular, the lift coefficient derivative with the stabilizer was decreased up to 99%. In addition, the sign change of $C_{m_{\delta e}}$ implied a complete oppsite phase lag of elevator control. Although the dynamic characteristics for the aircraft is still stable in the short period mode, the flight handling quality degraded to Level 3. The above results implied that the aircraft in atmospheric turbulence was difficult to control in the short period mode. This condition just lasted for several senconds. The above findings were consistent to the flight operation manual (FOM) for pilots. In FOM , the instructions for pilots, encountering the turbulence at high altitude, is that the elevator control should not be exercised. In this case, if the pilot applies the control force to the aircraft under severe turbulence, the unexpected delay and reversed control from elevator may occur and this may induce the PIO. This will cause much plunging and bumping when the aircraft flies through the turbulence.

Acknowledgment

This work is supported by National Science Council and Aviation Safety Council of Taiwan. The number of the project is: NSC97-3114-P-707-001-Y.

References

[1]Aviation Safety Council Aircraft Accident Report, "In-Flight Icing Encounter and Crash into the sea Transasia Airways Flight 791", Aprial, 2005.

[2]Eurocae working group 50, "Minimum Operational Performance Specification for Crash Protected Airborne Recorder Systems ED112", January 27, 2003.

[3]Iliff, Kenneth W., and Taylor Lawrence W, Jr, "Determination of Stability Derivatives from Flight Data Using a Newton-Raphson Minimization Technique", NASA H-626, 1972.

[4]Iliff, Kenneth W, 'Aircraft Parameter Estimation', NASA H-1394, 1987.

[5]Kenneth Hui, Lorenzo Auriti, and Joeseph Ricciardi, "Advances in Real-Time Aerodynamic Model Identification', *Journal of Aircraft* Vol.42, No.1, 2005, pp.73-79.

[6] Weng, C.T., Ho, C.S., Lan, C.E., and Guan M., "Aerodynamic Analysis of a Jet Transport in Windshear Encounter During Landing", *Journal of Aircraft*, Vol. 43, No. 2, 2006, pp. 419-427.

[7]Yang, M.H., Chang K.C, Guan M., Ho, C.S., Hsiao F.B.,"Applied flight data to analyse the aircraft encounter turbulence", *2006 AASRC/CCAS Joint Conference on Disk* [CD-Room], National Central University, Jhongli City.

[8]Appendix 1 of ICAO Doc 4444, "INSTRUCTIONS FOR AIR-REPORTING BY VOICE COMMUNICATIONS".
[9]Jack D. Mattingly, *Elements of Gas Turbine Propulsion*, McGraw-Hill, Inc., pp213-337, 1996.
[10]Suykens, Johan A. K./Moor, Bart L. R. de, *Artificial neural networks for modeling and control of non-linear systems*, Kluwer Academic Publishers, 1996.
[11]Gupta, Madan M., Jin, Liang., Homma, Noriyasu., *Static and dynamic neural networks :from fundamentals to advanced theory*, Wiley, 2003.
[12]Cook, M.V., Flight Dynamics Principles, Butterworth-Heinemann, Oxford, 1997, Chaps 2, 3, 4, 5, 6, 9, 10, 11.
[13]Robert C. Nelson, *Flight Stability and Automatic Control*, McGraw-Hill, Singapore, 1998, Chaps 3, 4.
[14]John. Hodgkinson, *Aircraft Handling Quality*, Blackwell Science Ltd, 1999, pp.54, 56.

AIAA Guidance, Navigation, and Control Conference
10 - 13 August 2009, Chicago, Illinois

AIAA 2009-6087

Nonlinear Filter Formulation for Rapid Estimation of Damaged Aircraft Performance

Jinwhan Kim*, Karthik Palaniappan†, and P. K. Menon‡
Optimal Synthesis Inc., Los Altos, CA 94022

Estimation of aerodynamic models of damaged aircraft using an innovative differential vortex lattice method tightly coupled with extended Kalman filters is discussed. The approach exploits prior knowledge about the undamaged aircraft to reduce the order of the estimation problem. Three different extended Kalman filter formulations are given, together with a comparative analysis. An approach for designing test maneuvers to improve the observability of the system dynamics is also discussed. Algorithms given in this paper can be used as the basis for online derivation of aircraft performance model, which can then form the basis for designing safe landing guidance laws for damaged aircraft.

I. Introduction

Adaptive control of damaged aircraft is being investigated at NASA and other aerospace research laboratories in the U.S.[1,2] The focus of these research efforts has been in maintaining control over the attitude dynamics of the damaged aircraft. Assuming that the aircraft remains controllable at its current flight conditions, it is important to be able to predict its performance at other flight conditions in order to derive maneuver constraints that should be enforced to ensure safe transition of the aircraft to landing configuration. The objective of the research discussed in this paper is to develop estimation schemes for rapidly extracting the aerodynamic parameters of damaged aircraft to enable the assessment of aircraft performance. The performance data of interest include flight envelope boundaries and maneuver limits. This data can form the basis for the design of safe landing guidance laws.

Several innovative concepts have been advanced in this paper. Firstly, a rapid approach for deriving aerodynamic models of damaged aircraft termed as the *Differential Vortex Lattice Method* (DVLM) was developed. This approach recasts the well known Vortex Lattice Method (VLM)[3] to reduce the dimension of the aerodynamic problem. The DVLM formulation exploits prior knowledge about the airframe to create a low-order computational methodology for relating the changes in the vehicle geometry due to damage to its aerodynamic parameters. This low-order method can be implemented in real-time onboard for the aircraft to provide estimates of the aerodynamic parameters for use in the computation of flight envelope and maneuver limits, and for adaptive guidance law synthesis. Approaches for estimating the maneuver limits and structural dynamic characteristics are also outlined.

Secondly, the Extended Kalman filtering (EKF) approach[4-6] is employed for online estimation of damaged aircraft parameters based on the DVLM. Design of maneuvers for enhancing the observability of the damaged aircraft model parameters is also discussed. The model parameters derived from the estimator can be used for computing the flight envelope and the maneuver limits. These can then be used in the synthesis of safe guidance laws for landing the aircraft.

Unlike the airframe stabilization problem, the guidance task is almost entirely based on predictive information about the aircraft dynamics. For instance, landing guidance requires the aircraft to slow down to the approach speeds while descending to the correct altitude at a specified heading. Since damaged aircraft may have a high drag and lower stall angle of attack, the aircraft energy has to be carefully managed to ensure that adequate lift is maintained until flare altitude and touchdown. This will require energy conservative maneuvers and descent strategies. Since damaged aircraft may not be able to employ all its high-lift devices, its speed must be carefully managed to avoid premature loss of lift. These factors make it important to derive a reasonably accurate performance model of the aircraft for the design of a viable guidance system. It may be noted that although most inner-loop flight control systems operate well within the limits of controllability most of the time, the guidance task often involves operating near the edges of the operational envelope.

* Research Scientist, 95 First Street, Suite 240, Senor Member AIAA.
† Research Scientist formerly at OSI, Currently with Amoeba Technologies Inc.
‡ Chief Scientist, 95 First Street, Suite 240, Associate Fellow AIAA.

This motivates the use of the indirect adaptive control framework[7] for the guidance problem, wherein an estimation procedure is used to find the parameters of the model, which then forms the basis for the design of guidance commands. Due to the use of predictive information available in the estimated model, this problem must be formulated carefully to ensure that the model closely approximates the expected dynamics of the damaged aircraft. This is because of the fact that due to their dependence on predictive information, guidance systems are much more susceptible to modeling uncertainties.

The present research assumes that the approximate location and extent of the damage on the airframe are known, perhaps from electro-optical sensors onboard the aircraft. Large modern aircraft may incorporate several cameras in the airframe, allowing rapid detection of any airframe anomalies.

Section II presents the equations of motion and the associated filter formulation. The differential vortex lattice method (DVLM) is described in Section III. The DVLM-based nonlinear filter formulations with various parameterization methods are given in Section II. The performance validation based on numerical simulations is presented in Section V, and the conclusions from the present research are given in Section VI.

II. Equations of Motion and Filter Formulation

The proposed approach for online estimation of damaged aircraft performance uses a nonlinear online estimation algorithm in conjunction with the Differential Vortex Lattice Method (DVLM). This paper focuses on investigating the feasibility of the proposed estimation algorithm. The 3D point-mass model is used for describing the motions of aircraft by assuming that the kinematic states of the aircraft are stabilized by the inner-loop controller. In this section, the equations of motion and the associated filter formulation are presented. Since the system dynamics is nonlinear, an Extended Kalman Filtering (EKF) algorithm is used in the filter formulation.

A. Point-Mass Dynamics of the Aircraft

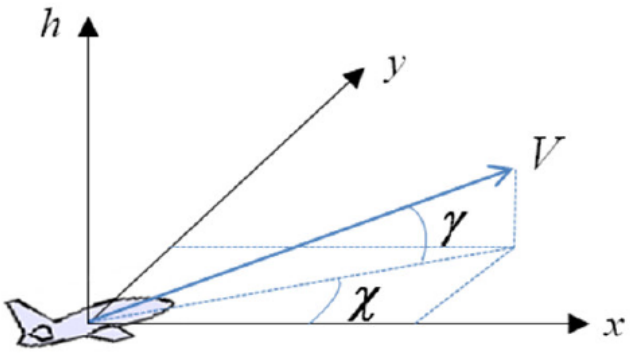

Figure 1. Coordinate system

The 3-D point-mass dynamics of an aircraft is used to describe the motion of aircraft in 3D configuration space. This model assumes that the control variables continuously maintain the aircraft moment equilibrium, such that the aircraft can follow commanded angle of attack α, angle of side slip β, and/or the bank angle ϕ. Based on the coordinate system shown in Figure 1, the equation of motion can be expressed in the form:

$$\dot{x} = \begin{bmatrix} \dot{V} \\ \dot{\gamma} \\ \dot{\chi} \\ \dot{x} \\ \dot{y} \\ \dot{h} \end{bmatrix} = \begin{bmatrix} (\eta T - D)/m - g\sin\gamma \\ (L\cos\phi - S\sin\phi)/(mV) - g\cos\gamma/V \\ (L\sin\phi - S\cos\phi)/(mV\cos\gamma) \\ V\cos\gamma\sin\chi \\ V\cos\gamma\cos\chi \\ V\sin\gamma \end{bmatrix} \tag{1}$$

In Equation (1), L is the lift, D is the drag, S the side force and T is the maximum thrust. The maximum thrust, T, is assumed to be constant. The actual thrust varies linearly with respect to the throttle setting η. Table 1 defines all the symbols used in Equation (1).

Table 1. Symbols used in the Equations of Motion

V	Velocity	Φ	Bank angle
γ	Flight angle	T	Thrust force
χ	Side-slip angle	L	Lift force
x	North	D	Drag force
y	East	S	Side force
h	Altitude	M	Mass
η	Throttle	g	Gravity acc.

B. Computing the Forces on a Damaged Aircraft using DVLM

Under normal operating conditions, the lift, drag, and side force in Equation (1) can be expressed as functions of aircraft geometry and aerodynamic parameters such as aircraft speed, angle of attack, and the angle of sideslip.

If physical damage occurs to the airframe, both the aircraft geometry and the aerodynamic parameters change, and thus the original relationships are no longer valid in describing the aerodynamic forces and the resulting motions. The Vortex Lattice Method (VLM) is capable of describing the aerodynamic forces based on the airframe geometry, and the distribution of circulation over discretized panels defining the geometric airframe can be calculated and integrated into forces at the given flight conditions, i.e.,

$$\begin{aligned} L &= L(\rho, \Gamma, A, V_\infty, \alpha, \beta) \\ D &= D(\rho, \Gamma, A, V_\infty, \alpha, \beta) \\ S &= S(\rho, \Gamma, A, V_\infty, \alpha, \beta) \end{aligned} \tag{2}$$

where ρ is the air density, Γ is the circulation strength distribution, A is the aircraft geometry, V_∞ is the airspeed, α is the angle of attack, and β is the angle of sideslip. Note that the circulation components are also functions of the aircraft geometry and the flight conditions. However, for the conventional VLM, the dimension of Γ is equal to the number of panels approximating the airframe, normally a large number. Designing online recursive estimators based on the VLM is unrealistic due to its high dimension.

The Differential Vortex Lattice Method (DVLM) proposed in this paper allows the calculation of the forces on the damaged aircraft using differential circulation strength components in the vicinity of the damaged section, involving a much smaller set of circulation strengths when compared with the conventional VLM approach. The associated reduction in the dimension allows the DVLM to be used as the basis for the derivation of recursive estimators.

C. EKF-based State-Parameter Estimation

The parameter estimation problem is often called the dual estimation problem since it requires the simultaneous estimation of the system states and the unknown parameters. In general, these problems involve system nonlinearities including nonlinear coupling between the states and the parameters. The extended Kalman filter (EKF) is most widely and commonly used for the formulation of nonlinear dual estimators. The implementation procedure of the EKF proceeds as follows:

For a given nonlinear system with unknown system parameters,

$$\dot{x} = f(x, \theta) + n_w \tag{3}$$

with x being the system state vector, θ the parameter vector to be estimated, and $f(\cdot)$ is the nonlinear function of states and parameters. The vector n_w is the process noise which is assumed to be Gaussian in the EKF development.

The dynamic model of the parameters θ is chosen based on any prior knowledge about its temporal behavior. The simplest model assumption is that θ is piecewise constant or $\dot{\theta} = 0$.

The augmented system dynamics can then be written as:

$$x^a = f^a(x,\theta) = \begin{bmatrix} \dot{x} \\ \dot{\theta} \end{bmatrix} = \begin{bmatrix} f(x,\theta) \\ 0 \end{bmatrix} + n_w^a \tag{4}$$

Here, x^a is the augmented system state vector.

Although θ is assumed to be piecewise constant, this model allows moderate time variations in the parameters through the artificial process noise vector n_w^a. The remaining filter design procedure is the same as that of the standard EKF implementation procedure outlined in Table 2.

Table 2. Extended Kalman Filter [4]

System model	$\dot{x} = f(x) + w$	$w \sim N(0, Q)$
Measurement model	$z_k = h_k(x_k) + v_k$	$v_k \sim N(0, R_k)$
Time propagation	$\dot{\hat{x}} = f(\hat{x})$ $\dot{P} = FP + PF^T + Q$	$F = \left[\frac{\partial f}{\partial x}\right]_{x=\hat{x}}$
Measurement update	$\hat{x}_k^+ = \hat{x}_k^- + L_k\left(z_k - h_k(x_k)\right)$ $P_k^+ = (I - L_k H_k) P_k^-$	$H_k = \left[\frac{\partial h_k}{\partial x}\right]_{x=\hat{x}_k^-}$ $L_k = P_k^- H_k^T \left(H_k P_k^- H_k^T + R_k\right)^{-1}$

For the present state-parameter estimation problem, the measurements, assumed to be available for the estimation process, are the aircraft position, velocity and acceleration components.

$$z = \begin{bmatrix} V & \gamma & \chi & x & y & h & \dot{V} & \dot{\gamma} & \dot{\chi} \end{bmatrix}^T + n_v^T \tag{5}$$

where n_v is the measurement noise vector.

III. Differential Vortex Lattice Method

A. Equations of Motion

The vortex lattice method (VLM) is based on inviscid, incompressible, steady and irrotational flow assumptions, and has proven to be highly effective for determining aerodynamic characteristics of the complete aircraft configurations[8-10]. Once the aerodynamic model has been determined, it can be used to predict the performance characteristics of the aircraft.

The first stage in the implementation of the vortex lattice method is the discretization of the vehicle geometry into vortex panels, as shown in Figure 2. The entire wing surface is divided into a number of vortex panels laid out in a lattice like structure. A horseshoe vortex with Circulation Γ is placed at the quarter-chord location of each panel. In the classical implementation of the vortex lattice method, the trailing vortices are assumed to extend to infinity. The wake is assumed to be flat. The control points are assumed to lie at the three quarter point of each panel.

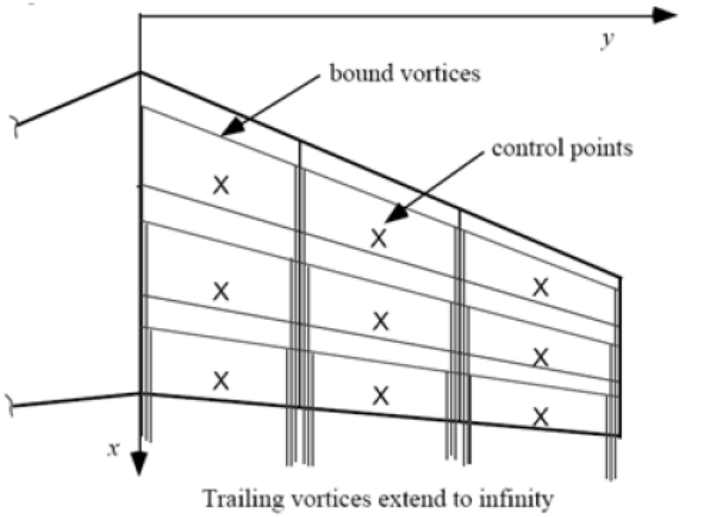

Figure 2. Discretization of a wing surface into vortex panels

The normal velocity at the control point of the m^{th} panel due to the horseshoe vortex at the n^{th} panel is given by

$$V_m = C_{m,n}\Gamma_n \tag{6}$$

Thus the normal velocity at the m^{th} control point due to all the vortices on the wing surface can be written as

$$V_m = \sum_{1}^{N} C_{m,n}\Gamma_n \tag{7}$$

The standard boundary condition imposed at any one of these control points ensures that the total normal ɔcity at any one of these control points is zero (i.e. no penetration boundary condition). This is enforced as ɔws:

$$V_m + V_\infty \sin(\alpha_m + \theta_m) = \sum_{1}^{N} C_{m,n}\Gamma_n + V_\infty \sin(\alpha_m + \theta_m) = 0 \tag{8}$$

Here, α_m and θ_m are the angle of attack and the local wing twist at the m^{th} control point. The parameters $C_{m,n}$ end on the geometry of the wing, and can be pre-computed. The above equation can then be written in matrix n as follows:

$$A\Gamma = b \tag{9}$$

Here, the matrix A depends only on the geometry of the wing, and can be pre-computed. The vector of boundary ditions b depends on the free-stream velocity V_∞, the local angle of attack α_m and the local wing twist θ_m. Γ is vector of circulation strengths of the horseshoe vortices.

Once the circulation strengths Γ are known, the total velocities $\vec{V}$ at the locations of the control points can be ɹulated as follows

$$\vec{V}_m = \vec{V}_\infty + \sum_{1}^{N} \vec{D}_{m,n}\,\Gamma_n \tag{10}$$

Bernoulli's equation can then be used to estimate the pressure at the control point locations as:

$$P_m = P_\infty + \frac{1}{2}\rho\left(V_\infty^2 - V_m^2\right) = P_m(\Gamma_i) \tag{11}$$

The forces along the x, y and z axes are then given respectively by

$$F_x = \sum_1^N P_n(\Gamma_i)dA_{n,x} \qquad F_y = \sum_1^N P_n(\Gamma_i)dA_{n,y} \qquad F_z = \sum_1^N P_n(\Gamma_i)dA_{n,z} \tag{12}$$

B. The Differential Vortex Lattice Method (DVLM)

The differential vortex lattice model investigated under the present research significantly reduces the dimension of the problem by exploiting the knowledge about the circulation over the aircraft structure before the damage. The DVLM problem is formulated in terms of computing the changes in the circulation on the panels in the neighborhood of the damage.

Let the circulation distribution over an undamaged wing be given by

$$A\Gamma = b \tag{13}$$

Here, Γ is the array containing the circulation strengths in the different panels, arranged in some pre-determined manner. The element a_{ij} of A represents the aerodynamic influence of the j^{th} panel on the i^{th} panel. It should be noted that

$$a_{ij} \propto \frac{1}{r_{ij}^2} \tag{14}$$

When a portion of the airframe is damaged, the circulation strength at that location can be assumed to go to zero. At this point, it is useful to note that the influence of the damaged panels is felt strongly only at the neighboring panels and can be considered insignificant sufficiently far away.

It is important to get a quantitative idea of the decay of the influence of the damaged panel. Consider a wing of span s, divided into n panels of the same size, span-wise. For the purposes of illustration, consider only one panel chord-wise. The size of each panel is then given by s/N. The distance between the control point of a panel and its periphery, where the bound vortex is assumed to be, is given by half this distance $s/(2N)$. The influence on a panel due to its own circulation is then given by

$$a_{i,i} \propto \frac{4N^2}{s^2} \tag{15}$$

The influence on a panel due to another panel, n panels away, is given by

$$a_{i,i+n} \propto \frac{N^2}{n^2 s^2} \tag{16}$$

The ratio of the influences is then given by

$$\frac{a_{i,i+n}}{a_{i,i}} = \frac{1}{4n^2} \tag{17}$$

It can be seen that the above equation is independent of the span s, and the total number of panels chosen N. If n is 3, then the ratio of influences is 2.77 percent, which can be considered quite small. Thus, if an error of 3 percent can be tolerated, it is sufficient to study flow over three panels adjacent to the damaged area on all sides. This has the advantage of reducing the area of computation of circulation strengths to 3 neighboring panels. Thus the elements of Γ_d are the same as those of Γ, except at locations 3 panels away in each direction from the location of damage.

Thus the equation for circulation can be rewritten as

$$\begin{bmatrix} A_{n1} & 0 & A_{n2} \\ 0 & 0 & 0 \\ A_{d1} & 0 & A_{d2} \end{bmatrix} \begin{bmatrix} \Gamma_n \\ 0 \\ \Gamma_d + \delta\Gamma \end{bmatrix} = \begin{bmatrix} b_n \\ 0 \\ b_d \end{bmatrix} \tag{18}$$

where the subscript n represents undamaged values and d represents damaged values. The vector $\delta\Gamma$ represents the change in circulation between damaged and undamaged values. The expression for $\delta\Gamma$ then becomes:

$$\delta\Gamma = A_{d2}^{-1}\left(b_d - A_{d1}\Gamma_n\right) - \Gamma_d \tag{19}$$

This is the fundamental hypothesis of the Differential Vortex Lattice Method (DVLM). The process of formulating the differential circulation is illustrated in Figure 3.

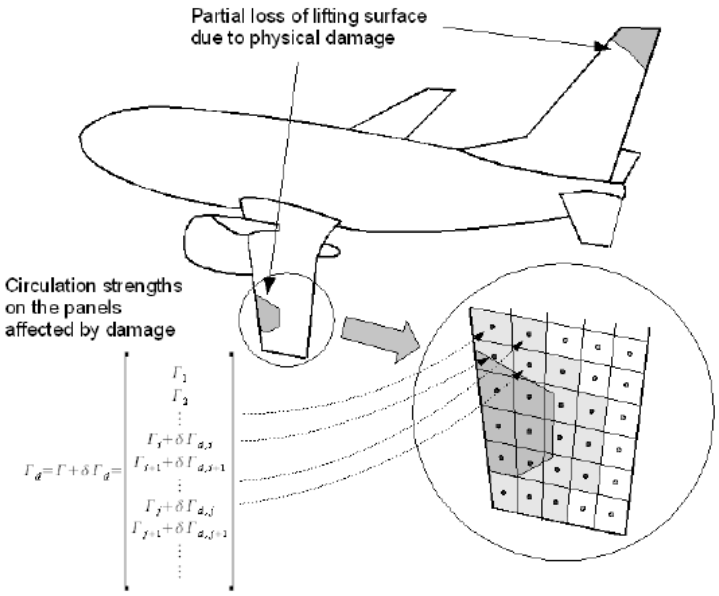

Figure 3. Modeling airframe damage using Differential Vortex Lattice Method

The corrected circulation vector can be used to evaluate the pressure distribution of the damaged airframe. The pressure distribution can be integrated to produce aerodynamic forces. The aerodynamic forces can then be normalized with respect to dynamic pressure and reference area to yield drag, lift and side force coefficients. The Differential Vortex Lattice Method is summarized in Figure 4.

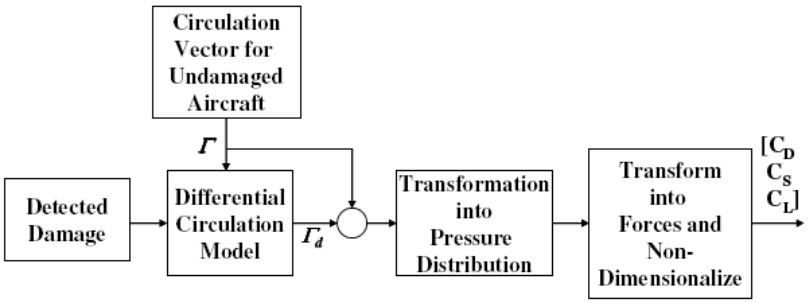

Figure 4. A Summary of the Differential Vortex Lattice Method

IV. DVLM-based EKF Formulations

This section will discuss two DVLM-based EKF formulations with different sets of parameter states. These are:

- *Circulation Strength Estimation* : Circulation strength distributions are introduced as the system parameters to be estimated. Two variations of this estimation problem will be discussed.

- *Parameterized Damage Estimation* : The extent of damage is directly estimated by an appropriate parameterization of the damage.

Details of these two approaches are presented in the following subsections.

A. Formulation 1: Direct Estimation of the Differential Circulation Vector

The filter is initialized with the pre-computed undamaged aircraft circulation strength vector and the measured state vector. Given the aircraft position, velocity and acceleration vectors derived from GPS/INS system and air data sensors onboard, the EKF will generate estimates of the differential circulation vector and the resulting aerodynamic coefficients. The overall structure of the proposed estimator, together with a potential closed-loop guidance system, is given in Figure 5.

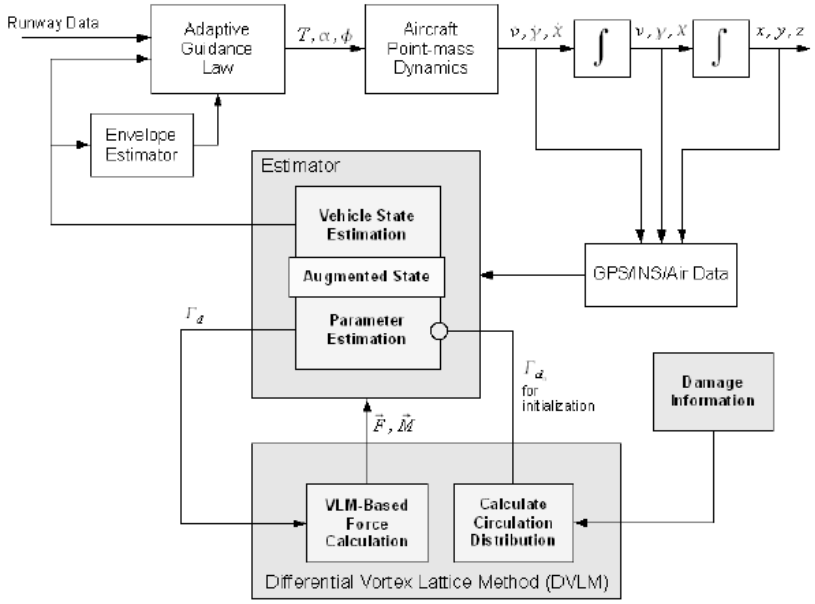

Figure 5. Filter structure for circulation strength estimation

The augmented system dynamics for the state-parameter estimation problem can be written as follows:

$$\dot{x}^a = \begin{bmatrix} \dot{V} \\ \dot{\gamma} \\ \dot{\chi} \\ \dot{x} \\ \dot{y} \\ \dot{h} \\ \delta\dot{\Gamma}_1 \\ \delta\dot{\Gamma}_2 \\ \vdots \\ \delta\dot{\Gamma}_m \end{bmatrix} = \begin{bmatrix} (\eta T - D)/m - g\sin\gamma \\ (L\cos\varphi - S\sin\varphi)/(mV) - g\cos\gamma/V \\ (L\sin\varphi - S\cos\varphi)/(mV\cos\gamma) \\ V\cos\gamma\sin\chi \\ V\cos\gamma\cos\chi \\ V\sin\gamma \\ -\zeta_1\delta\Gamma_1 \\ -\zeta_2\delta\Gamma_2 \\ \vdots \\ -\zeta_m\delta\Gamma_m \end{bmatrix} + n_w^a \qquad (20)$$

Here, n_w^a is the process noise vector.

The associated Jacobian matrix for the augmented system dynamics, F^a, can be expressed as:

$$F^a = \frac{\partial f^a}{\partial x^a} = \left[\begin{array}{c|c} A \in R^{6\times 6} & B \in R^{6\times m} \\ \hline 0 \in R^{m\times 6} & diag(\varsigma_i) \in R^{m\times m} \end{array}\right] \tag{21}$$

The partitioned matrix A involves the partial derivatives of force components with respect to the speed, L_V, D_V and S_V which can be calculated by numerical differentiation. The force sensitivities to the changes in circulation components, L_Γ, D_Γ and S_Γ involved in the partitioned matrix B can be evaluated inside the DVLM solver, which reduces the computational load. Two different perturbation models for the differential circulation strength estimator were formulated. Based on the magnitude of expected changes in the estimated differential circulation strengths, these are termed as the heavy and light perturbation models.

Heavy perturbation model

The state vector $\delta\Gamma_i$, is the perturbation term defined as

$$\Gamma_{d,i} = \Gamma_{u,i} + \delta\Gamma_i \tag{22}$$

where Γ_u is the circulation vector for the undamaged case, and Γ_d is for the damaged case. Note that this formulation attempts to estimate the entire differential circulation strength vector. To achieve a better filter performance, first-order Markov processes are employed for the differential circulation states. A small leakage constant ζ is introduced to improve the condition of the estimation problem. If ζ is set to zero, $\delta\Gamma$ follows a standard Wiener process.

Light perturbation model

The second differential approach attempts to determine the changes in the differential circulation strength vector defined as:

$$\Gamma_{d,i} = \Gamma_{d,i}^{DVLM} + \delta\Gamma_i \tag{23}$$

In this case, the circulation strength vector for the damaged case is calculated using the DVLM, and the perturbation of this circulation strength vector is estimated using the EKF. This reduces the absolute magnitude of the perturbation by exploiting the DVLM more effectively, perhaps leading to a better estimation performance.

This procedure requires the DVLM solver to run at each time step, and is computationally more intensive than the heavy perturbation approach. However, the computational requirements of DVLM approach are modest, enabling its use in the EKF algorithm.

B. Formulation 2: Estimator based on Parameterized Description of the Damage

The second formulation is based on damage parameterization in which the parameter state represents the size or extent of damage. The filter directly estimates the actual size of the damage using sensor measurements, and the DVLM algorithm provides circulation strength solutions and the resulting forces on the airframe. This approach has several advantages over the circulation estimation approach given previously.

Firstly, the filter is robust to initial error and the uncertainty in the initial damage estimate determined from sensors, since the damage size is directly estimated by the filter. Secondly, the damage parameterization generally involves a much smaller number of parameter states when compared with the number of circulation states. This reduces the number of state variables to be estimated, improving the system's observability and estimator performance.

The major limitation of this damage estimation approach is that the DVLM module has to be run at each time step. Moreover, sufficient accuracy is required for the DVLM solver since its output is directly used for the subsequent force evaluation without being updated by sensor measurements. In order to improve the accuracy, the original DVLM solver is modified using the Gauss Seidel smoothing procedure that incurs a slight increase in computational cost.

However, various numerical experiments during the present research have revealed that the proposed approach can provide higher accuracy with improved computational efficiency. Figure 6 gives the structure of the estimator. Note that this is a slightly modified version of the estimator given in Figure 5. The filter employs the sensor measurements in conjunction with the forces computed from the DVLM solver to update the damage parameter state. As stated in Introduction, it is assumed that information required for parameterizing the damage is available from onboard electro-optical sensors.

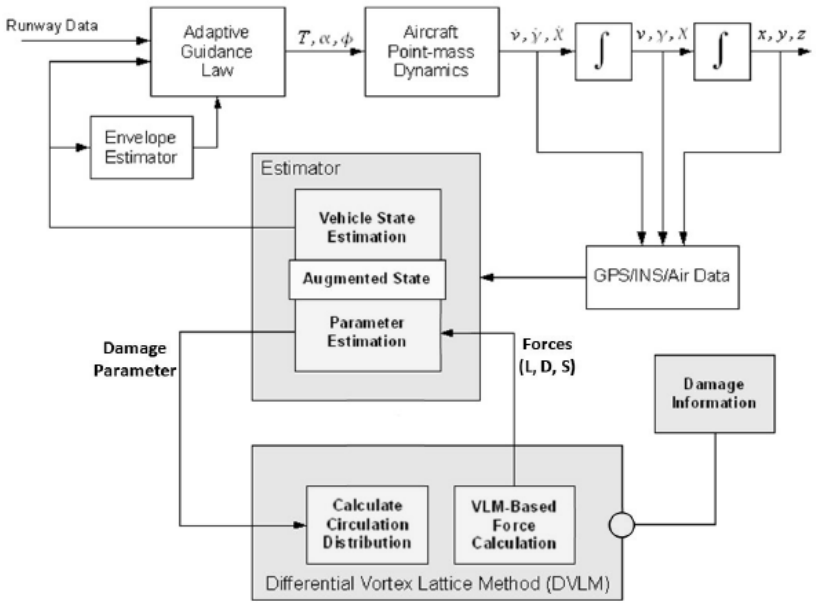

Figure 6. Filter structure for parameterized damage estimation

The augmented system state for state-parameter estimation can be expressed by

$$\dot{x}^a = \begin{bmatrix} \dot{V} \\ \dot{\gamma} \\ \dot{\chi} \\ \dot{x} \\ \dot{y} \\ \dot{h} \\ \dot{\theta}_1^d \\ \vdots \end{bmatrix} = \begin{bmatrix} (\eta T - D)/m - g\sin\gamma \\ (L\cos\phi - S\sin\phi)/(mV) - g\cos\gamma/V \\ (L\sin\phi - S\cos\phi)/(mV\cos\gamma) \\ V\cos\gamma\sin\chi \\ V\cos\gamma\cos\chi \\ V\sin\gamma \\ -\zeta_1\theta_1^d \\ \vdots \end{bmatrix} + n_w^a \tag{24}$$

Here θ^d are the damage parameters. The Jacobian matrix for the system dynamics can be represented as

$$F^a = \frac{\partial f^a}{\partial x^a} = \left[\begin{array}{c|c} A = \dfrac{\partial f}{\partial x} \in R^{6\times 6} & f_\theta = \dfrac{\partial f}{\partial \theta} \in R^{6\times Dim(\theta)} \\ \hline 0 \in R^{Dim(\theta)\times 6} & diag(\zeta_i) \end{array}\right] \tag{25}$$

The partitioned Jacobian matrix f_θ needs to be evaluated numerically due to the complexity of the relationship between damage parameterization and the system dynamics.

In fact, the damage parameterization can be done in various ways. A parameterization scheme using a single scalar damage parameter is employed in the present research. Specifically, the number of damaged panels, which is a direct measure of the damaged area, is used as a parameter state. Illustrative examples of the parameter numbering schemes depending on damage configurations are shown in Figure 7 and Figure 8.

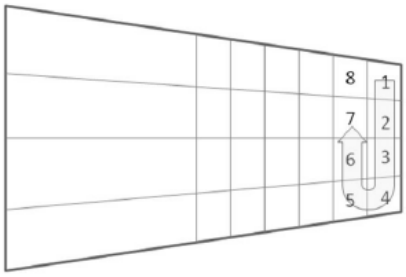

Figure 7. Tip damage parameterization

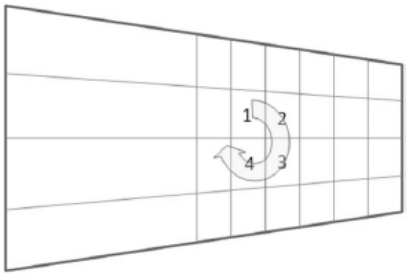

Figure 8. Hole damage parameterization

V. Simulation Results and Performance Analysis

A series of numerical simulations are set up to evaluate the performance of the state-parameter estimation methods discussed in this chapter. The full VLM is used for simulating the actual aircraft dynamics, and the DVLM-based EKF formulations are used for online estimation of aircraft states and parameters.

A. Simulation Scenarios

The two following damage configurations are considered for the present simulations.

Case 1 : Wing-tip damage

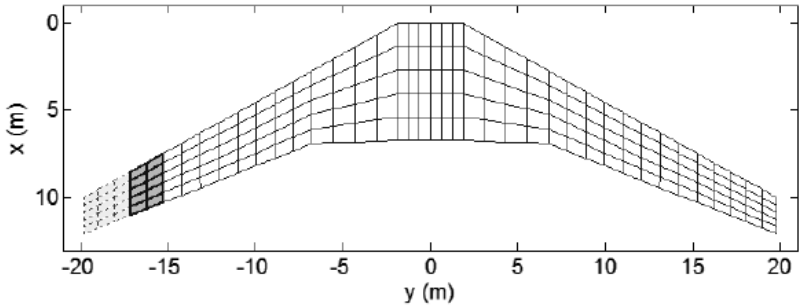

Figure 9. Damage configuration (case 1): Total number of panels = 200, number of damaged panels = 15, number of panels for DVLM analysis = 10

Case 2 : Hole-in-the-wing damage

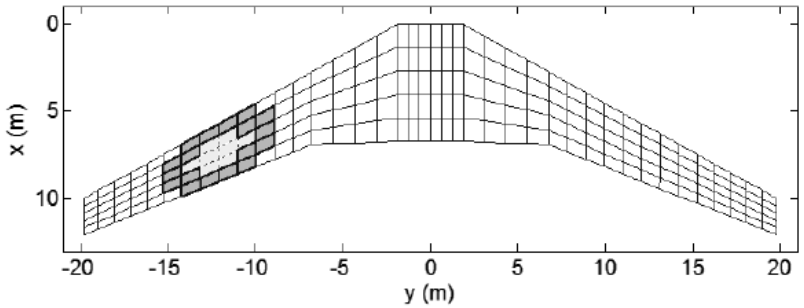

Figure 10. Damage configuration (case 2): Total number of panels = 200, number of damaged panels = 8, number of panels for DVLM analysis = 18

Note that term *damage* in this paper implies the loss of lifting surface panels on which the circulation strengths are zero.

Simulation settings are given in Table 3.

Table 3. Simulation parameter settings

Parameter	Value
Aircraft weight	45941 (kgf)
Nominal thrust	5791 (N)
Nominal angle of attack	6º
Initial Speed	130 (nm/hr)
Initial Altitude	3000 (m)
Process noise covariance	diag(0,0,0,0,0,0,1,…,1)
Measurement noise covariance	diag(0.1^2, 0.00175^2, 0.00175^2, 1.0^2, 1.0^2, 1.0^2, 1.0^2, 0.0175^2, 0.0175^2)

B. Information-Enhancing Input Design

Oscillatory inputs in angle of attack, angle of sideslip and bank angle are used as the information-enhancing inputs. The amplitudes of these inputs are determined based on sensitivity analysis, and the excitation frequency and simulation time span are chosen based on the period of the Phugoid mode [11]. Figure 11 illustrates the control input histories used to generate the results given in this chapter.

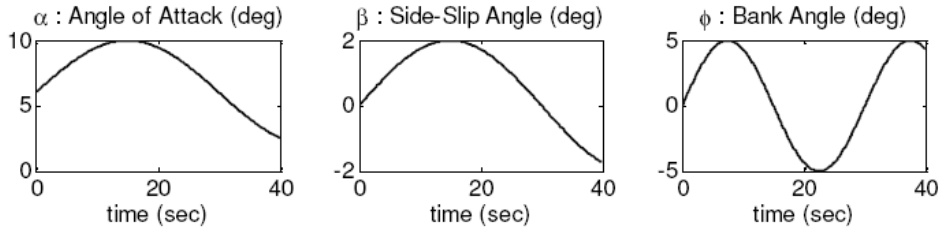

Figure 11. Aircraft inputs used in the simulation

For the present simulations, the angle of attack starts from the nominal equilibrium value of 6º for the undamaged aircraft.

C. Simulation Results

Perturbation models in Equations (22) and (23) are used in the estimation algorithm for the two damage scenarios. It is assumed here that 15 panels are damaged in the wing-tip damage configuration, and 8 panels in the hole-in-the-wing damage configuration. The dimension of the circulation state vector varies depending on the damage configuration for the filter based on Formulation 1. In order to construct the circulation state vector for this approach, 10 panels are used for the wing-tip damage configuration, and 18 panels for the hole-in-the-wing damage configuration.

Figure 12 and Figure 13 show the motion state estimate errors for the wing-tip damage scenario and the hole-in-the-wing damages scenario, respectively. For each damage scenario, the error histories of the three estimators, two for Formulation 1 and one for Formulation 2, are plotted to enable a quantitative comparison between them. In the

figures, the solid blue lines and the dashed green lines correspond to the DVLM estimators based on Formulation 1, and the dotted red lines are the error histories from the parameterized damage estimator based on Formulation 2.

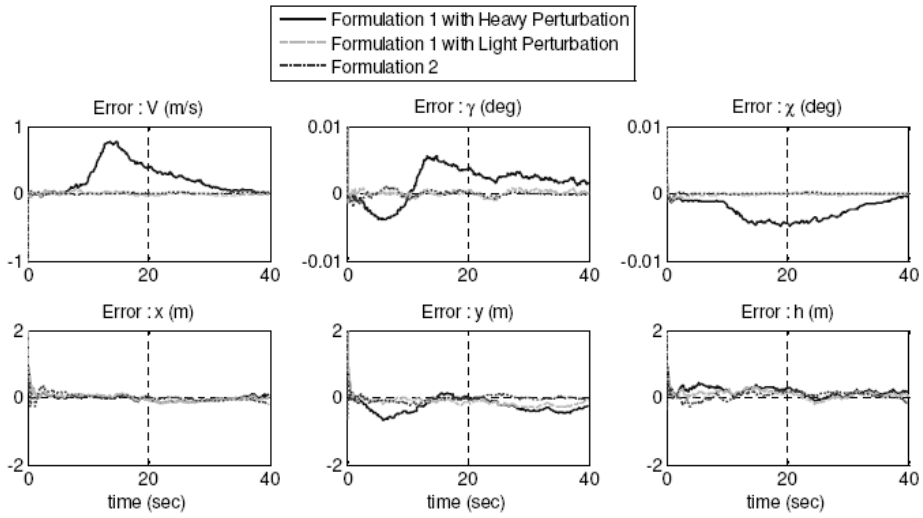

Figure 12. Errors in the aircraft motion state estimates (wing-tip damage)

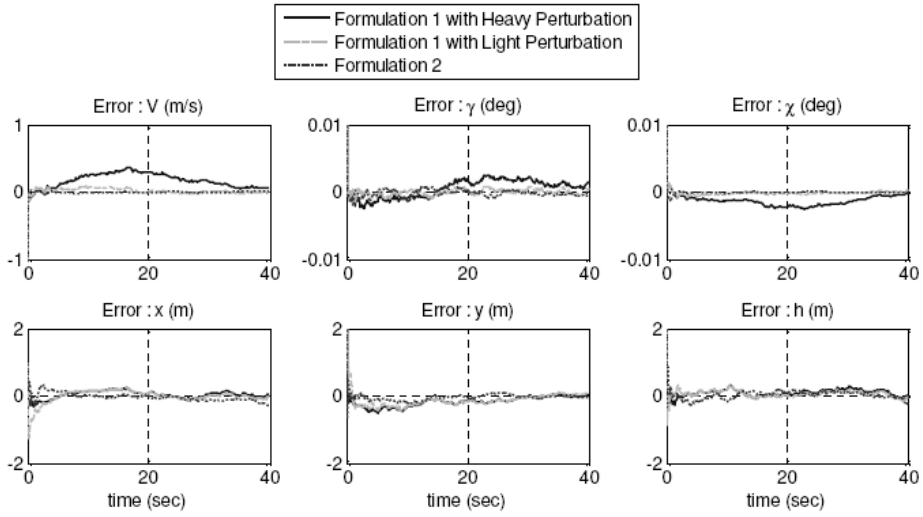

Figure 13. Errors in the aircraft motion state estimates (hole-in-the-wing damage)

All the proposed formulations show satisfactory performance for the aircraft motion state estimates. In particular, excellent filter performance is observed for Formulation 1 with light perturbation and Formulation 2. This is mainly because of the availability of direct measurements for all those motion states in the measurement equation shown in Equation (5).

However, their performances in estimating unmeasured states and resulting aerodynamic forces greatly vary depending on the formulations and perturbation models. The results for the wing-tip damage and the hole-in-the-wing damage scenarios are shown in Figure 14 and Figure 15.

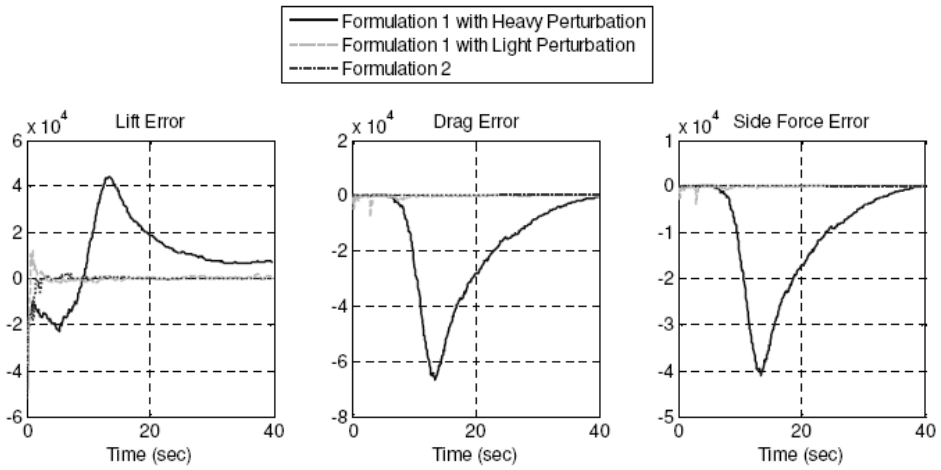

Figure 14. Errors in the aerodynamic force estimates (wing-tip damage)

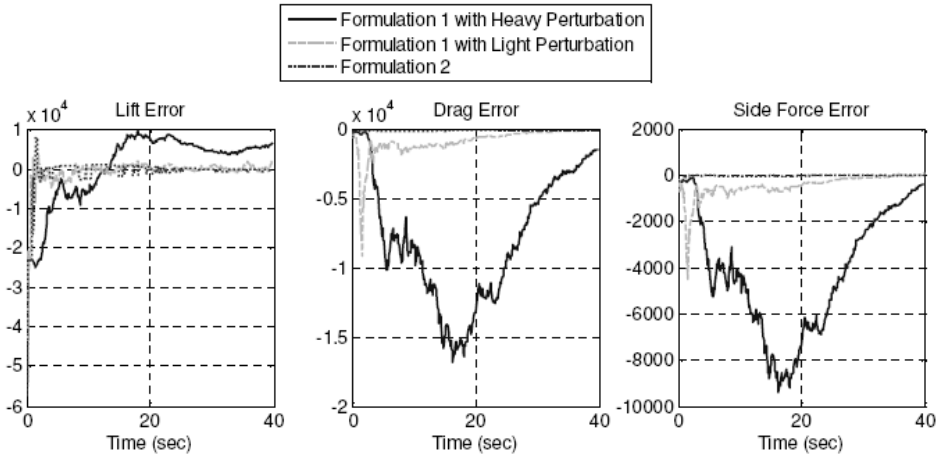

Figure 15. Errors in the aerodynamic force estimates (hole-in-the-wing damage)

Regarding Formulation I, the filter with light perturbation outperforms the heavy perturbation filter. The performance of the heavy perturbation model is inadequate. The leakage constant provides artificial system damping and prevents the filter from diverging, however the filter with heavy perturbation basically lacks numerical stability. The light perturbation model employs smaller corrections and uses more information from the DVLM solver, and shows improved performance considering the system's marginal observability and the minor inaccuracies in the DVLM. In fact, this observation led to the conjecture that using the DVLM as an open loop solver and focusing on improving the accuracy of inputs to the DVLM solver might provide better overall performance, which resulted in the second formulation with direct damage parameterization.

As can be observed in the above figures, the second formulation provides excellent filter performance. In addition to the accurate estimation of the aircraft states, good force estimation results are obtained as shown in Figure 14 and Figure 15. The state estimate for the number of damaged panels for the hole-in-the-wing damage configuration is shown in Figure 16. Figure 17 compares the associated circulation strengths and the results by the full VLM formulation.

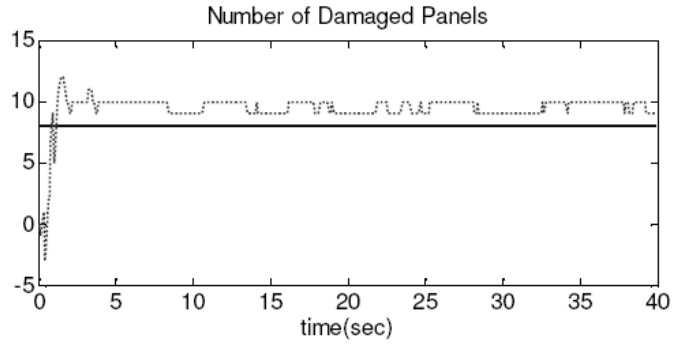

Figure 16. Estimate of the number of damaged panels

(Formulation 2, hole-in-the-wing damage)

Figure 16 shows that the estimate converges within a few seconds, however steady state errors remain. This error is due to the difference between the full VLM and DVLM formulations. The error can be reduced by improving the accuracy and fidelity of the DVLM algorithm.

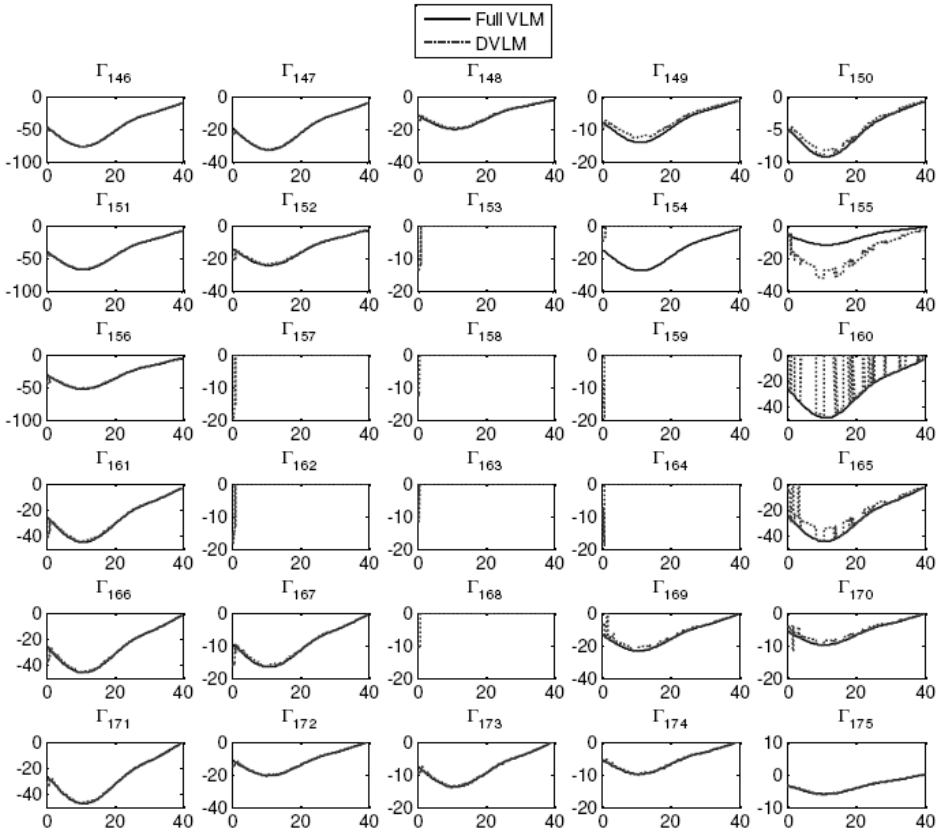

Figure 17. Circulation vector estimates: VLM vs DVLM+EKF

(Formulation 2, hole-in-the-wing damage)

For the hole-damage, the panels with the ID numbers *153*, *157, 158, 159*, *162, 163, 164*, and *168* are the damaged panels on which circulation strengths are zero, and the adjacent panels are the boundary panels. Some errors and ambiguities are observed near the boundaries of the damage due to the errors in the estimation of the number of damaged panels and the approximation algorithm by the DVLM algorithm. However, the overall estimation performance appears to be very satisfactory. In particular, it is observed that the circulation strength prediction errors based on the estimated parameter are quite localized. Another advantage of this formulation is that the filter dimension and its convergence rate are not explicitly dependent on the resolution of the airframe geometric discretization used in formulating the DVLM.

The following observations can be made from these plots:

- The filter using DVLM Formulation 1 with the light perturbation model and the filter using Formulation 2 with the parameterized damage outperform the filter using the DVLM Formulation 1 with the heavy perturbation.
- The filter using Formulation 2 shows the best force estimation performance among the three proposed approaches, especially during the transient phase.

Table 4 summarizes the performance comparison between the three approaches proposed in this paper.

Table 4. Performance Summary

Filter Formulation	**Formulation 1** (Circulation Strength Estimation)		**Formulation 2** (Parameterized Damage Estimation)
	Heavy Perturbation	Light Perturbation	
Parameter State	$\delta\Gamma_i$ $\left(=\Gamma_{u,i}-\Gamma_{d,i}\right)$	$\delta\Gamma_i$ $\left(=\Gamma_{d,i}^{DVLM}-\Gamma_{d,i}\right)$	θ_i (Damage Size)
State-dimension Scalability	Poor	Poor	Good
Dependency on DVLM	Low	Moderate	High
Overall Computational Cost	Low ~ Moderate	Moderate ~ High	Moderate
Estimation Accuracy	Poor	Good	Good
Filter Stability and Robustness	Poor	Fair	Good

VI. Concluding Remarks

This paper described extended Kalman filter algorithms based on a differential vortex lattice method to realize a practical approach for determining the aerodynamic model of a damaged aircraft, and to use it as the basis for estimating flight constraints. The present research was motivated by the desirability of relating the damaged aircraft geometry with its flight dynamics. Central premises involved in the research are that the inner-loop flight control system allows the continued flight of the aircraft, onboard sensors can provide information about the location and qualitative nature of the damage on the airframe, and that the Vortex Lattice method can provide sufficiently accurate aerodynamic characterization of the aircraft.

A novel, computationally efficient algorithm for computing the aerodynamic forces on damaged aircraft, termed as the Differential Vortex Lattice Method (DVLM), was advanced in this paper. This algorithm uses prior knowledge of the aerodynamic model to derive a differential formulation of the well-known Vortex Lattice Method. It was shown that the algorithm is accurate, and can provide several orders of magnitude savings in computational

time when compared with the Vortex Lattice Method. The computationally efficient differential formulations make it possible to rapidly estimate the aerodynamic model of damaged aircraft, and use it eventually for designing safer landing guidance algorithms.

The differential vortex lattice algorithm was then used as the basis for the design of three extended Kalman filters. Using a point-mass dynamic model, these estimators were shown to be capable of extracting the damaged aircraft aerodynamic parameters from the motion measurements. Accurate estimation of the aircraft motion and the aerodynamic parameters using the extended Kalman filters was demonstrated in two distinct damage simulations. Numerical simulations were performed to demonstrate and compare the performance of the proposed filtering algorithms. The results confirm that Formulation 2 based on the direct damage parameterization outperforms the other approaches which estimate circulation strengths.

Acknowledgments

This research was supported under NASA SBIR Contract No. NX08CA50P, with Ms. Diana Acosta of NASA Ames Research Center serving as the Technical Monitor. We thank Dr. K. Krishnakumar and Dr. Nhan Nguyen of NASA for their interest and support of this research.

References

[1] Nguyen, N., Krishnakumar, K., Kaneshige, J., and Nespeca, P., "Flight Dynamics and Hybrid Adaptive Control for Stability Recovery of Damaged Asymmetric Aircraft," Journal of Guidance, Control, and Dynamics, Vol. 31, No. 3, pp. 751-764, 2008.

[2] Rysdyk, R.T. and Calise, A.J., "Fault Tolerant Flight Control via Adaptive Neural Network Augmentation," AIAA Guidance, Navigation, and Control Conference, Boston, MA. 1998.

[3] Kuethe, A. M., and Chow, C-Y, *Foundations of Aerodynamics*, Wiley, New York, NY, 1998.

[4] Gelb, A., *Applied Optimal Estimation*, MIT Press, Cambridge, MA, 1989.

[5] Bar-Shalom, Y., Li X. R. and Kirubarajan, T., *Estimation with Applications to Tracking and Navigation*, John Wiley & Sons, 2001.

[6] Jazwinski, A. H., *Stochastic Processes and Filtering Theory*, Academic Press, New York, NY, 1970.

[7] Astrom, K. J., and Wittenmark, B., *Adaptive Control*, Addison-Wesley, Menlo Park, CA, 1989.

[8] Melin, T., "A Vortex Lattice MATLAB Implementation for Linear Aerodynamic Wing Applications," Master's Thesis, Department of Aeronautics, Royal Institute of Technology (KTH), Stockholm, Sweden, 2000.

[9] Magnus, A. E. and Epton, M. A., *PAN AIR-A Computer Program for Predicting Subsonic or Supersonic Linear Potential Flows About Arbitrary Configurations Using A Higher Order Panel Method*, Vol. 1. Theory Document (Version 1.0), NASA CR-3251, 1980.

[10] Miranda, L. R., Elliott, R. D., and Baker, W. M., "A Generalized Vortex Lattice Method for Subsonic and Supersonic Flow Applications," NASA CR-2865, 1977.

[11] Blakelock, J. H., *Automatic Control of Aircraft and Missiles*, John Wiley & Sons, 1991.